

# Thermal Hall transport in extended Kitaev models

Tsuyoshi Okubo,<sup>1,2</sup> Joji Nasu,<sup>3,2</sup> Takahiro Misawa,<sup>4,5</sup> and Yukitoshi Motome<sup>6</sup>

<sup>1</sup>*Institute for Physics of Intelligence, University of Tokyo, Tokyo, 113-0033, Japan*

<sup>2</sup>*JST, PRESTO, Saitama, 332-0012, Japan*

<sup>3</sup>*Department of Physics, Tohoku University, Sendai 980-8578, Japan*

<sup>4</sup>*Beijing Academy of Quantum Information Sciences, Haidian District, Beijing 100193, China*

<sup>5</sup>*Institute for Solid State Physics, University of Tokyo,*

*5-1-5 Kashiwanoha, Kashiwa, Chiba 277-8581, Japan*

<sup>6</sup>*Department of Applied Physics, University of Tokyo, Tokyo, 113-8656, Japan*

The thermal Hall conductivity—a thermal current analog of the Hall conductivity for electric current—is a useful detector for exotic particles, such as the Majorana particles. For example, the half-integer quantization of the thermal Hall conductivity at the zero temperature limit has been regarded as direct evidence of the Majorana particles. However, it has not been clarified how the thermal Hall conductivity behaves at finite temperatures even for the celebrated Kitaev model on a honeycomb lattice, which is one of the basic models for realizing the Majorana particles in quantum magnets. Here, using a state-of-the-art tensor network method, we investigate how the thermal Hall conductivity behaves in the Kitaev model with additional interactions under a magnetic field. We find that the thermal Hall conductivity significantly exceeds the value of the half-integer quantization in the intermediate temperature range, which is consistent with the experimental result of  $\alpha\text{-RuCl}_3$ . We also find that the field-angle dependence of the thermal Hall conductivity is consistent with the sign of the Chern number of the Majorana particles. We demonstrate that the additional off-diagonal interactions (namely,  $\Gamma$  and  $\Gamma'$  terms) largely affect the thermal Hall conductivity. In particular, we show that negative  $\Gamma'$  and positive  $\Gamma$  terms remarkably enhance the amplitude of the thermal Hall conductivity at the intermediate temperature region. We also analyze a classical limit of the extended Kitaev model that ignores quantum effects as a counterpart of quantum systems. From the comparison between the classical systems and the quantum systems, we find that the effects of the  $\Gamma'$  term can be captured by the classical model while the effects of the  $\Gamma$  term cannot. This indicates that the quantum effects of the  $\Gamma$  term are significant. Our comprehensive analysis of the thermal Hall conductivity in the extended Kitaev model provides a firm basis for understanding the half-integer quantization of the thermal Hall conductivity in the Kitaev materials such as  $\alpha\text{-RuCl}_3$ .

## I. INTRODUCTION

Quantum spin liquids (QSLs) are enigmatic states of quantum spins, which do not show any symmetry breaking even at zero temperature. Since the QSLs are the source of exotic emergent particles, such as Majorana particles anyons, the search for QSLs has been one of the central issues of modern condensed matter physics. Among several QSLs, the Kitaev QSL [1], which appears as the ground state of the Kitaev model on the honeycomb lattice, has attracted a great deal of attention because it has been rigorously shown that noninteracting Majorana particles appear in low-energy degrees of freedom. However, it has been a challenging problem how to detect the Majorana particles in the Kitaev QSL, since the Majorana particles are neutral and do not show any characteristic behaviors as a response to electric or magnetic fields.

The thermal Hall conductivity is a promising quantity for detecting the emergent Majorana particles as they carry heat [1]. In the Kitaev model, perturbatively-introduced magnetic fields make the Majorana fermion systems topologically nontrivial. Accordingly, a chiral edge current appears, which is protected by the Chern number. Because the chiral edge current is an energy current of Majorana fermions, the thermal Hall conduc-

tivity takes the half-quantized value

$$\frac{\kappa_{xy}}{T} = \frac{1}{2} \frac{\pi k_B^2}{6\hbar} \quad (1)$$

in the zero temperature limit. This half-quantization offers direct evidence of the Majorana particles.

Recently, a thermal Hall experiment for  $\alpha\text{-RuCl}_3$  proposed that the half-quantization of the thermal Hall conductivity occurs under a tilted magnetic field [2]. Although  $\alpha\text{-RuCl}_3$  shows magnetic zigzag-order at zero magnetic field [3–5], inelastic neutron scattering measurements suggested that applying magnetic fields induces the Kitaev QSL [6]. The observed half-quantized thermal Hall conductivity indicates that topologically nontrivial Majorana bands emerge in the Kitaev candidate material  $\alpha\text{-RuCl}_3$  under a magnetic field. Similar half-quantized thermal Hall conductivities were observed under in-plane magnetic fields [7]. It is also shown that the angular dependence of the thermal Hall conductivity on the magnetic field is consistent with those in the Kitaev model [8]. Independent measurement of the thermal Hall conductivity also shows the half-integer quantization of the thermal Hall conductivity [9].

However, there remains controversy on interpreting the observed thermal Hall transport as the evidence of the Kitaev QSL. For example, the observed thermal Hall con-

ductivity shows an overshoot of the half-quantized value for higher temperatures, and the origin of such overshooting behaviors has not been resolved while contributions from phonons [10, 11] and visons [12] have been proposed. In addition, real compounds, including  $\alpha$ -RuCl<sub>3</sub>, could contain additional interactions such as the Heisenberg interactions [13, 14], and the off-diagonal  $\Gamma$  and  $\Gamma'$  interactions [15–17]. The effect of such additional interactions to the thermal Hall conductivity beyond the perturbation theories [18, 19] is not fully clarified yet.

Furthermore, several later experiments for  $\alpha$ -RuCl<sub>3</sub> discussed relationship to the quantum oscillations observed in the longitudinal thermal conductivity [20], the topological magnons[21], the para-magnon[22], the phonons[23]. The origin of the thermal Hall conductivity has not been settled. To resolve the origin of the thermal conductivity observed in experiments, it is demanding to perform unbiased analysis of the thermal Hall conductivity of the Kitaev model and its extensions without assuming any quasiparticle excitations.

Although the thermal Hall transport in the pure Kitaev model has been well understood in the limit of zero temperature and weak magnetic fields, which are introduced by perturbation expansions [1], the accurate analysis of the thermal Hall conductivity under magnetic field beyond the perturbation theory is limited. For finite temperature properties, we may use Monte Carlo simulation for zero magnetic field [24, 25]. These calculations successfully showed a double-peak structure in specific heat and its relationship to the Majorana fermions. Unfortunately, however, in order to treat finite magnetic fields necessary for thermal Hall transport, we need to consider an effective interaction justified only for sufficiently small magnetic fields to avoid negative sign problems [26]. Numerical simulations on the effective model showed non-monotonic temperature dependence of the thermal Hall conductivity: it has a weak peak at high temperature and converges to the half-quantized value [26]. However, the peak value is much smaller than the half-quantized value, and then, the huge  $\kappa_{xy}$  beyond the half-quantized value, which is observed in the experiment of  $\alpha$ -RuCl<sub>3</sub>, has not been explained by the effective model based on the perturbation theory.

The effect of the symmetric off-diagonal interactions, called  $\Gamma$  and  $\Gamma'$  terms, have also been investigated based on the perturbative treatment justified in the situation of small magnetic fields and small off-diagonal interactions [18, 19]. In the case of  $\Gamma'$  interactions, it was shown that the  $\Gamma'$  introduces an additional contribution to the gap of Majorana-fermion band [18]. The total gap is increased (decreased) for the negative (positive)  $\Gamma'$  interaction. Thus, the finite-temperature behaviors of the thermal Hall conductivity might largely depend on the sign of  $\Gamma'$ . Based on the similar perturbation theory, Ref. [19] discussed that the effect of the  $\Gamma$  interaction appeared as the third-order contribution. Although it indicates that the effect of  $\Gamma$  in the thermal Hall transport is less than that of  $\Gamma'$ , the same analysis also showed a pos-

sible quantum phase transition induced by the effective interaction from the third-order perturbation. Therefore, non-trivial effect may be induced by the phase transitions. Note that, as we mentioned, these analyses are based on the perturbation theory justified for small  $\Gamma$  and  $\Gamma'$ . Furthermore, the connections to the thermal Hall transport are only discussed within the zero temperature limit. Thus, to understand the effect of the off-diagonal interactions at finite temperatures, it is necessary to perform analysis beyond the perturbation theory.

As the origin of the thermal Hall transport at finite temperatures, we can also consider topological magnons excited from the magnetic order induced by the applied magnetic fields [27, 28]. The edge modes due to such topological magnons exist with a nonzero gap and then the corresponding thermal Hall transport becomes zero in the zero temperature limit. However, at finite temperatures, we need to consider a contributions from such topological magnons in addition to the contributions from the Majorana fermions. In realistic situations, the thermal Hall transport might not be solely explained by the Majorana fermions or the topological magnons. To understand the thermal Hall transport at a finite temperature, we need an unbiased method that can treat a complicated mixture of these contributions.

In this paper, we investigate the thermal Hall transport in the extended Kitaev models, which include the off-diagonal interactions, by the finite-temperature tensor network method and the approach exploiting the thermal pure quantum states. For comparison, we also perform the classical Monte Carlo simulations for the classical limit of the extended Kitaev models. We properly define the energy current from the model Hamiltonian and calculate the edge current in the systems with open boundaries. This treatment does not assume any origins of the thermal Hall transport, and considers all contributions on equal footing. We find that this calculated thermal Hall conductivity shows clear overshooting behavior similar to the experimental observations, indicating that the experimentally observed thermal Hall conductivity might be explained by the simple extended Kitaev models. We also discuss the effect of off-diagonal interactions on the thermal Hall conductivity. Indeed, we find that depending on the sign and the type of the off-diagonal couplings, the thermal Hall conductivity can change its sign at finite temperature.

The organization of this paper is as follows. In Sec. II, we introduce the extended Kitaev model and give a brief overview of previous studies on the extended Kitaev model. In Sec. III, we explain how to calculate the thermal Hall conductivity for the extended Kitaev model. We also explain the methods used in this study, i.e., the exponential tensor renormalization (XTRG) method, the thermal pure quantum state (TPQ) method, and the classical Monte Carlo simulation. In Sec. IV A, we show the temperature dependence of the thermal Hall conductivity for the pure Kitaev model under a magnetic field along [111] direction. We also show the field-angle de-

pendence of the thermal Hall conductivity. In Sec. IV B, we show how the off-diagonal interactions  $\Gamma$  and  $\Gamma'$  terms affects the temperature dependence of the thermal Hall conductivity. In Sec. IV C, we analyze thermal Hall conductivity in the classical limit of the Kitaev model. Section V is devoted to a summary and discussion.

## II. MODEL

To investigate the thermal Hall transport in Kitaev systems, we consider an extended Kitaev model containing the off-diagonal  $\Gamma$  and  $\Gamma'$  interactions on the honeycomb lattice (Fig. 1). The Hamiltonian of the model under a magnetic field is given as

$$\mathcal{H} = \sum_{\gamma=x,y,z} \sum_{\langle i,j \rangle_\gamma} \mathcal{H}_{ij}^\gamma - \sum_{i,\gamma} h^\gamma S_i^\gamma, \quad (2)$$

with

$$\mathcal{H}_{ij}^\gamma = \left[ KS_i^\gamma S_j^\gamma + \Gamma (S_i^\mu S_j^\nu + S_i^\nu S_j^\mu) + \Gamma' (S_i^\mu S_j^\gamma + S_i^\nu S_j^\gamma + S_i^\gamma S_j^\mu + S_i^\gamma S_j^\nu) \right] \quad (3)$$

$$= \sum_{\alpha,\beta=x,y,z} J_{\alpha\beta}^\gamma S_i^\alpha S_j^\beta, \quad (4)$$

where  $\langle i,j \rangle_\gamma$  means the nearest neighbor pair on the  $\gamma$ -bond.  $(\mu, \nu, \gamma)$  represents a cyclic permutation of  $(x, y, z)$ , for example,  $(\mu, \nu, \gamma) = (y, z, x)$  for the  $x$ -bond.

The off-diagonal symmetric spin interactions with  $\Gamma$  and  $\Gamma'$  were first introduced in Ref. [15] as additional contributions to the Kitaev and Heisenberg interactions. These interactions are given as superexchange-type couplings between nearest neighbor  $j_{\text{eff}} = 1/2$  spins in transition metal ions with strong spin-orbit coupling where neighboring octahedra consisting of ligand ions share their edges. They are derived by performing perturbation expansions in the strong correlation limit of the three orbital Hubbard model for the  $t_{2g}^5$  configuration [29]. The virtual hoppings via  $p$  orbitals in ligand ions mainly dominate the exchange process, and direct hoppings between the neighboring  $d$  orbitals are secondary. The former induces the Kitaev and  $\Gamma$  interactions, but the Heisenberg interaction is caused only by the latter. Hence, the Kitaev and  $\Gamma$  interactions are believed to be leading interactions for governing the magnetic properties in Kitaev candidate materials [17, 30, 31]. The  $\Gamma'$  interaction does not appear in the case where the octahedra surrounding transition metal ions retain the cubic symmetry. The symmetry lowering by a trigonal distortion, which is inevitable in real materials, results in this interaction [15]. The spin excitations and thermodynamic properties of extended Kitaev models including  $\Gamma$  and  $\Gamma'$  interactions have been calculated and realistic parameters have been examined to reveal the magnetic properties of the Kitaev candidate materials, iridium oxides  $A_2\text{IrO}_3$  ( $A = \text{Na}, \text{Li}$ ) and  $\alpha\text{-RuCl}_3$  [32–35]. Most theoretical works suggested

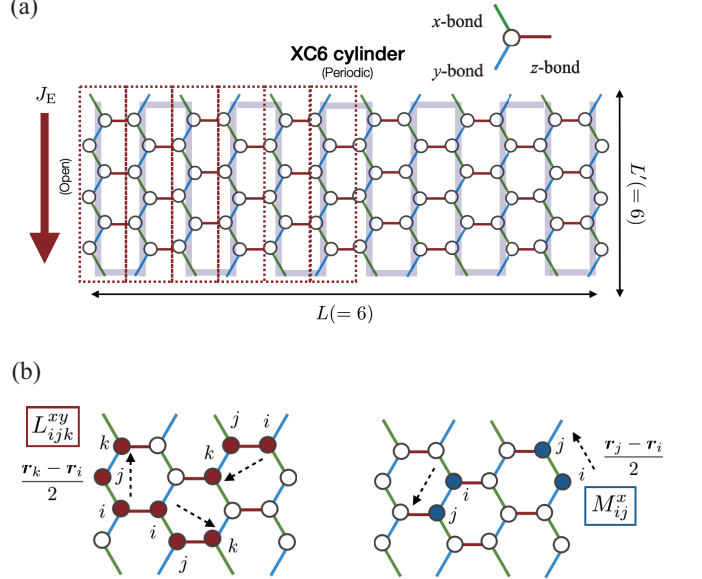


FIG. 1. (a) Schematic view of an  $(L, L') = (6, 6)$  honeycomb lattice structure consisting of 72 sites. Along the vertical direction, we impose the periodic boundary condition, while the open boundary condition is imposed in the horizontal axis. We consider the thermal current  $J_E$  in a downward direction indicated by the arrow. In the tensor network simulation, we consider a snake-like matrix product operators indicated by the gray thick line behind the lattice. (b) Graphical representations of the three-body ( $L$ ) and the two-body ( $M$ ) terms in the definition of the thermal current (6).

$K < 0$  and  $\Gamma > 0$  for  $\alpha\text{-RuCl}_3$  but the sign of  $\Gamma'$  is still under debate.

Because of the complexity of realistic models, the  $K\text{-}\Gamma$  model has been studied recently as a simplified model. This model has been examined by using the exact diagonalization [36, 37], Density Matrix Renormalization Group (DMRG) method [38], tensor network [39, 40], variational approach [41], spin-wave theory [42], and classical spin approach [43]. In the  $K\text{-}\Gamma$  model, there is large degeneracy in the classical limit. Once quantum fluctuations are taken into account, quantum-disordered states could potentially emerge, but the detailed phase diagram is still controversial. The introduction of the  $\Gamma'$  interaction to the  $K\text{-}\Gamma$  model with  $K < 0$  and  $\Gamma > 0$  brings about ordered phases in addition to quantum-disordered states. It has been pointed out that a ferromagnetic phase and chiral spin phase with nonzero spin scalar chirality appear in the case with  $\Gamma' > 0$  [44, 45]. On the other hand, the negative  $\Gamma'$  induces the zigzag order, which has been observed in Kitaev-candidate materials at low temperatures [39, 46–48]. Thus, this model might be suitable to investigate the relevant effect of off-diagonal interaction on the thermal Hall conductivity in real compounds including  $\alpha\text{-RuCl}_3$ .

Throughout the paper, we consider the ferromagnetic Kitaev interaction  $K = -1$ , which is naturally expected

from the superexchange process in  $t_{2g}^5$  systems. We also set the amplitude of the primitive translation vector of the honeycomb lattice to the unit length and  $k_B = \hbar = 1$ . We discuss, typically, physical quantities for the model on  $(L, L') = (6, 6)$  shown in Fig. 1(a). The total system size is given by  $N_s = 2 \times L \times L'$ . In Appendix A, we compare the results with those of  $(L, L') = (4, 8)$ .

### III. METHOD

In this section, we introduce the definition of the thermal Hall conductivity for finite-size clusters described above. Then, we explain numerical methods for calculating the finite temperature properties of the model. To investigate quantum spin models, we employ two methods. For smaller clusters, we use the thermal pure quantum state (TPQ) method, while we employ a tensor network-based method for larger clusters. As a reference to the quantum model, we investigate the classical spin model with the same interaction coefficients by using the Monte Carlo simulations.

#### A. Thermal Hall conductivity

To investigate the thermal Hall conductivity in the Kitaev systems, we first define the energy polarization  $\mathbf{P}_E$ , which are defined as [26, 49]

$$\mathbf{P}_E = \sum_{\alpha, \beta, \gamma} \sum_{\langle i, j \rangle_\gamma} \frac{\mathbf{r}_i + \mathbf{r}_j}{2} J_{\alpha\beta}^\gamma S_i^\alpha S_j^\beta - \sum_{i, \gamma} \mathbf{r}_i h^\gamma S_i^\gamma, \quad (5)$$

where  $\mathbf{r}_i$  is the position of the site  $i$ . From the commutation relation between the Hamiltonian and  $\mathbf{P}_E$ , the energy current  $\mathbf{J}_E$  is defined as

$$\mathbf{J}_E = i [\mathcal{H}, \mathbf{P}_E] = \sum_{\gamma, \gamma'} \sum_{\langle i, j, k \rangle_{\gamma, \gamma'}} \frac{\mathbf{r}_k - \mathbf{r}_i}{2} L_{ijk}^{\gamma\gamma'} + \sum_{\gamma} \sum_{\langle i, j \rangle_\gamma} \frac{\mathbf{r}_j - \mathbf{r}_i}{2} M_{ij}^\gamma, \quad (6)$$

where  $\langle i, j, k \rangle_{\gamma, \gamma'}$  represent the three neighboring sites consisting of the two nearest-neighbor pairs  $\langle i, j \rangle_\gamma$  and  $\langle j, k \rangle_{\gamma'}$  connected at site  $j$ . The operator  $L_{ijk}^{\gamma\gamma'}$  is the contribution from three-spin correlations,

$$L_{ijk}^{\gamma\gamma'} = \sum_{\alpha, \beta, \alpha', \beta', \gamma''} J_{\alpha\beta}^\gamma J_{\alpha'\beta'}^{\gamma'} \epsilon_{\alpha\gamma''\alpha'} S_i^\beta S_j^{\gamma''} S_k^{\beta'}, \quad (7)$$

and  $M_{ij}^\gamma$  represents the contribution from two-spin correlations,

$$M_{ij}^\gamma = \sum_{\alpha, \beta, \gamma', \gamma''} J_{\alpha\beta}^\gamma h_{\gamma'} \epsilon_{\gamma'\alpha\gamma''} (S_i^{\gamma''} S_j^\beta - S_i^\beta S_j^{\gamma''}), \quad (8)$$

where  $\epsilon_{\alpha\beta\gamma}$  means the completely antisymmetric tensor, which comes from the commutation relation between

spins. It is worth noting that three product of spin operators in  $L_{ijk}^{\gamma\gamma'}$  coincides with the effective field derived by third-order perturbations with respect to  $\hbar$  [26]. In the Majorana representation, the the effective field gives next nearest-neighbor hoppings, which opens excitation gaps in noninteracting Majorana fermion bands and results in topologically non-trivial band structures with nonzero Chern numbers [1]. Thus, the chiral edge current originating from  $L_{ijk}^{\gamma\gamma'}$  is expected to appear and contribute to the thermal Hall effect at least in the pure Kitaev model with weak magnetic fields.

We note that our definition of the energy current is different from that used in Ref. [50], where the energy current is defined by the commutation relation between the local Hamiltonians. Since the energy current in the system should be defined by the commutation relation between the total Hamiltonian and the total energy polarization, Eq. (6) should be a proper definition of the energy current. The energy current used in Ref. [50] might drop non-local contributions to the energy current. This might be the reason why  $\kappa_{xy}$  in Ref. [50] is significantly smaller than that shown in this paper.

Here, we introduce the energy current  $J_{E,l}^{\parallel}$  along the zigzag chain labeled by line  $l$  such that  $J_{E,l}^{\parallel}$  includes the contributions from the local currents on the segments inside the box surrounding the chain and across its right edge, which are shown in Fig. 1 (a). Note that due to the symmetry of the system,  $J_{E,\text{all}}^{\parallel} = \sum_{l=1}^L J_{E,l}^{\parallel}$  is exactly zero for any temperatures. To pick up contribution to the thermal Hall current from  $J_E^{\parallel}$ , we consider that each term in Eq.(6) represents the current density at  $(\mathbf{r}_i + \mathbf{r}_j)/2$  and sum them up from the left edge to the center of the system, which is defined as

$$J_E^{\parallel} = \sum_{l=1}^L J_{E,l}^{\parallel}. \quad (9)$$

By taking the derivative of  $J_E^{\parallel}$  with respect to the temperature, we obtain the thermal Hall conductivity as

$$\kappa_{xy} = \frac{2}{L'} \frac{d\langle J_E^{\parallel} \rangle_T}{dT}, \quad (10)$$

where  $\langle J_E^{\parallel} \rangle_T$  represents the thermal average at a temperature  $T$ , and  $L'$  is the length along the circumferential direction of the cylinder (Fig. 1(a)).

#### B. Tensor network method

In this section, we explain the tensor network method used in our study. To calculate finite-temperature properties of the model, we approximate a density matrix of the system at an inverse temperature  $\beta$ ,  $\rho(\beta) = e^{-\beta\mathcal{H}}$ , as a matrix product operator (MPO) with the bond dimension  $D$  [See Fig. 2(a)]. The string of the MPO is arranged in a snake form as shown in the gray line in Fig. 1 (a).

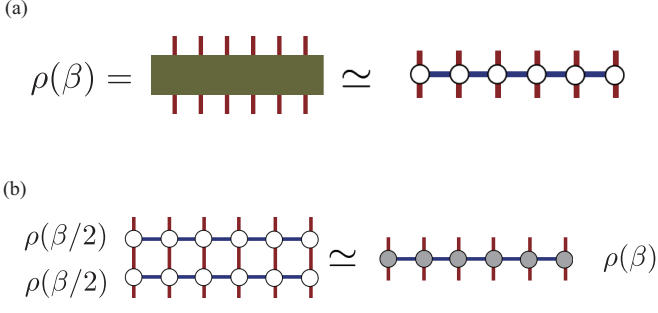


FIG. 2. Tensor network diagram for the density operator approximation. (a) The density matrix is approximated as a matrix product operator with bond dimension  $D$ . Here, the horizontal line corresponds to the gray line in Fig. 1(a). (b) The density matrix at  $\beta$  is calculated as  $\rho(\beta) = \rho(\beta/2)\rho(\beta/2)$ . The bond dimension of the obtained  $\rho(\beta)$  is truncated to  $D$  through the standard optimization procedure of MPS.

To optimize the tensors in an MPO as the density matrix at  $\beta$ , we employ the exponential thermal tensor renormalization group (XTRG) approach [51, 52], which has successfully calculated finite temperature properties of the Kitaev model [52]. In the XTRG method, we calculate the density matrix at  $\beta$  through the relationship

$$\rho(\beta) = \rho(\beta/2)\rho(\beta/2). \quad (11)$$

When  $\rho(\beta/2)$  is represented by MPO with the bond dimension  $D$ ,  $\rho(\beta)$  becomes an MPO with the bond dimension  $D^2$ . We approximate  $\rho(\beta)$  by MPO with  $D$  through the standard optimization procedure for the matrix product states (MPS) [51] [see Fig. 2(b)]. In particular, we employ the two-site update, and the computation cost of the XTRG method scales as  $O(D^4)$ . As the initial condition of the XTRG method, we prepare  $\rho(\beta_0)$  with  $\beta_0 = 10^{-7}$  through the approximated form  $\rho(\beta_0) \simeq 1 - \beta_0 \mathcal{H}$ , where the Hamiltonian is represented as an MPO. We calculate the expectation value of an operator  $O$  through thus obtained  $\rho(\beta)$  as  $\langle O \rangle = \text{Tr} [O\rho]/\text{Tr} \rho$  (Note that the density matrix is not normalized). The temperature derivative of  $\langle O \rangle$  is computed through numerical derivative.

In the following, we mainly show the data with  $D = 500$  for  $(L, L') = (6, 6)$  cylinder. Several benchmark calculations for different  $D$  and a different lattice shape are shown in Appendix A.

### C. Thermal pure quantum state

In this section, we explain the basics of the canonical thermal pure (cTPQ) state method [53], which enables us to calculate the finite temperature properties of quantum many-body systems using the power method. We note that several similar methods were independently proposed [54–57] before the proposal of

the cTPQ method [53]. We construct the cTPQ state  $|\Phi_{\text{cTPQ}}^p\rangle$  as follows:

$$|\Phi_{\text{cTPQ}}^p(\beta)\rangle = \exp\left[-\frac{\beta}{2}\mathcal{H}\right]|\Phi_{\text{rand}}^p\rangle, \quad (12)$$

where  $\beta$  is inverse temperature and  $|\Phi_{\text{rand}}^p\rangle$  is the  $p$ th initial random vector, which uniformly distributed on the  $N_H$  dimensional hypersphere ( $N_H$  is the dimension of the Hilbert space of the given system). Any local physical quantities at inverse temperature  $\beta$  can be calculated as the expectation values of  $|\Phi_{\text{cTPQ}}^p(\beta)\rangle$ , i.e.,

$$\langle A(\beta) \rangle = \frac{\langle \Phi_{\text{cTPQ}}^p(\beta) | A | \Phi_{\text{cTPQ}}^p(\beta) \rangle}{\langle \Phi_{\text{cTPQ}}^p(\beta) | \Phi_{\text{cTPQ}}^p(\beta) \rangle}. \quad (13)$$

We numerically construct the cTPQ state as follows:

$$\exp\left[-\frac{\beta}{2}\mathcal{H}\right]|\Phi_{\text{rand}}^p\rangle = U(\Delta\tau)^k|\Phi_{\text{rand}}^p\rangle, \quad (14)$$

$$U(\Delta\tau) = \exp\left[-\frac{\Delta\tau}{2}\mathcal{H}\right] \sim \sum_{n=0}^{n_{\max}} \frac{1}{n!} \left(-\frac{\Delta\tau}{2}\mathcal{H}\right)^n, \quad (15)$$

$$\beta = k\Delta\tau, \quad (16)$$

where we take  $n_{\max} = 6$  and  $\Delta\tau = 0.02$  in this paper. We confirm that  $n_{\max} = 6$  ( $\Delta\tau = 0.02$ ) is sufficiently large (small) for obtaining converged physical quantities in the calculated temperature region. In actual calculations, we use  $\mathcal{H}\Phi$  [58–60], where the cTPQ method is implemented.

The cTPQ method gives the numerically exact results within the statistical fluctuations, which are defined by the statistical distribution of the initial random vectors. To evaluate the fluctuations, i.e., the errors of the cTPQ method, we employ the bootstrap method [cite a standard textbook]. The benchmark result of the cTPQ method in the pure Kitaev model is shown in Appendix B. We also show the comparison between the XTRG method and the cTPQ method in Appendix C.

### D. Classical Monte Carlo simulation

Finally, we show the details of the classical Monte Carlo simulations. In this method, an  $S = 1/2$  spin at each site is regarded as a classical vector. Namely, a classical spin at site  $i$  is parameterized by  $\theta_i$  and  $\phi_i$  as  $\mathbf{S}_i = \frac{1}{2}(\sin \theta_i \cos \phi_i, \sin \theta_i \sin \phi_i, \cos \theta_i)$ . In the calculation of the thermal average, the integral  $\int \prod_i d\phi_i d\theta_i \sin \theta_i$  is evaluated by using the Markov-chain Monte Carlo method. To accelerate the computation speed and avoid trapping the spin configuration at local minima, we use the replica exchange method [61]. In the simulations, we prepare 48 replicas with different temperatures. We perform 10 000 000 MC steps for measurement after 10 000 MC steps for thermalization in the 800-site cluster with  $L = 10$  and  $L' = 40$  [see Fig. 1(a)]. The temperature derivative of  $\langle O \rangle$  is evaluated by the correlation with  $\mathcal{H}$  as  $d\langle O \rangle / dT = (\langle A\mathcal{H} \rangle - \langle A \rangle \langle \mathcal{H} \rangle) / T^2$ , while it is computed as a numerical difference in the case of the quantum system.

## IV. RESULT

### A. Pure Kitaev model

#### 1. Magnetic field along [111] direction

We first discuss temperature dependence of the physical quantities including the thermal Hall conductivity  $\kappa_{xy}$  of the ferromagnetic Kitaev model under a magnetic field parallel to [111] direction. In this setup, we expect positive  $\kappa_{xy}$  for small magnetic fields  $h = |\mathbf{h}|$  in the zero temperature limit [1].

Fig. 3(a)–3(c) shows the temperature dependence of the specific heat  $C$ , the magnetic moment along the magnetic field  $M_{\parallel}$ , and the flux density  $W$ , which are defined as

$$C = \frac{\langle \mathcal{H}^2 \rangle - \langle \mathcal{H} \rangle^2}{T^2} \quad (17)$$

$$M_{\parallel} = \langle \mathbf{M} \rangle \cdot \frac{\mathbf{h}}{|\mathbf{h}|}, \quad \mathbf{M} = \frac{1}{N_s} \sum_i \mathbf{S}_i \quad (18)$$

$$W = \frac{1}{N_h} \sum_p \langle W_p \rangle, \quad W_p = 2^6 \prod_{i \in p} S_i^{\gamma_i}, \quad (19)$$

where  $p$  runs all hexagons in the honeycomb lattice and  $N_h$  is the number of hexagons.  $\gamma_i$  represents the bond component not belonging to the edges of  $p$  at site  $i$ .

As shown in Fig. 3(a), we find that clear double peak structures appear at each magnetic field, which is a characteristic behavior of the Kitaev model [24, 25]. By increasing the magnetic field, we find that the low-temperature peaks move to higher temperatures while the high-temperature peaks are almost independent of the magnetic field. This tendency is understood from the local flux degrees of freedom are sensitive to the magnetic field. (三澤さんへ：後半の文が正しいか判断できませんでした。少し直感に反している気もします。)

At low magnetic field ( $h \lesssim 0.03$ ), we find that non-smooth temperature dependencies appear in the specific heat at low temperatures. The origin of these non-smooth behaviors might be the effects of the finite bond dimensions. However, for  $h \gtrsim 0.04$ , the temperature dependence of the specific heat is smooth down to  $T = 0.01$ . Therefore, it is plausible that  $D = 500$  is sufficient to discuss the thermal properties of the Kitaev model under magnetic field. Additional discussions on the bond-dimension dependencies are shown in Appendix A.

We next discuss the temperature dependence of the magnetization and the flux density. As expected, by increasing the magnetic field, the magnetic moment monotonically increases and it reaches more than 60% of the saturation value of magnetization at  $h = 0.08$  and  $T = 0.01$ . Since an applied magnetic field inducing nonzero magnetization renders a flux operator on each hexagonal plaquette nonconserved quantity, the flux density monotonically decrease by increasing the magnetic field. At  $h = 0.08$ , the flux density  $W$  is about 0.4 at low

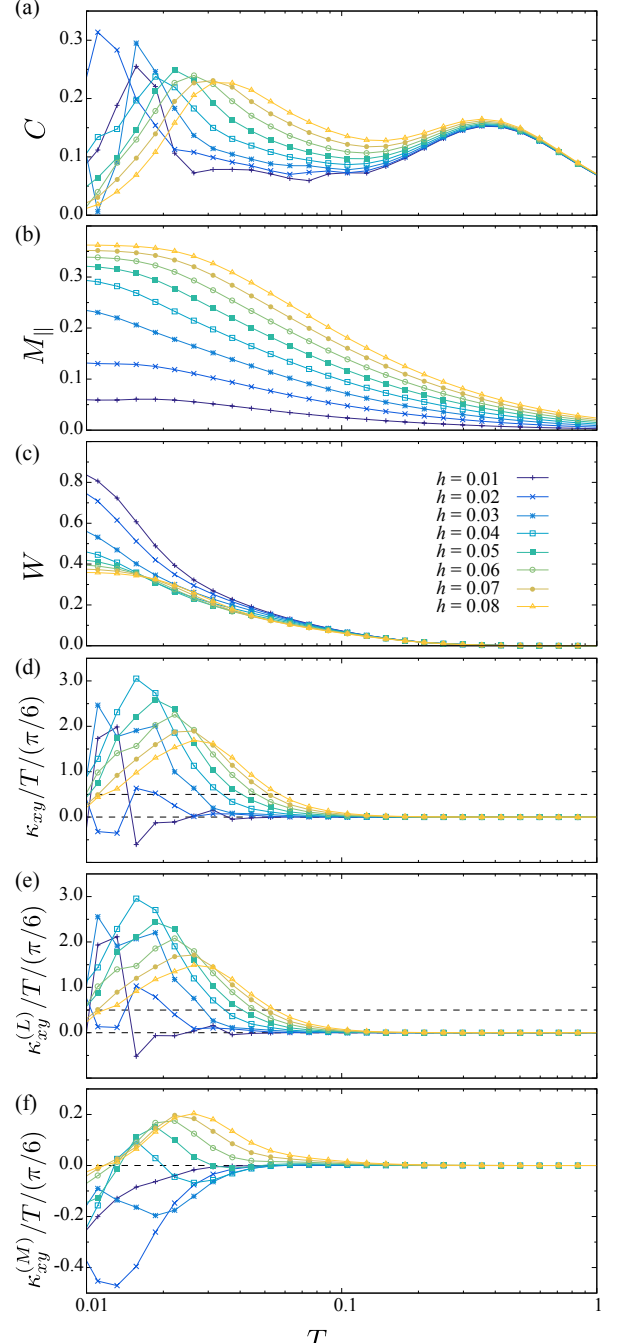


FIG. 3. Temperature dependence of (a) the specific heat (b) the magnetic moment (c) the flux, and (d)  $\kappa_{xy}/T$  of the ferromagnetic Kitaev model for various external magnetic field parallel to the [111] direction. (e,f) Contributions from the three-body ( $L$ ) and the two-body ( $M$ ) terms to  $\kappa_{xy}/T$ , respectively. Two horizontal dashed lines indicate  $\kappa_{xy}/T = 0$  and the half-quantized value.

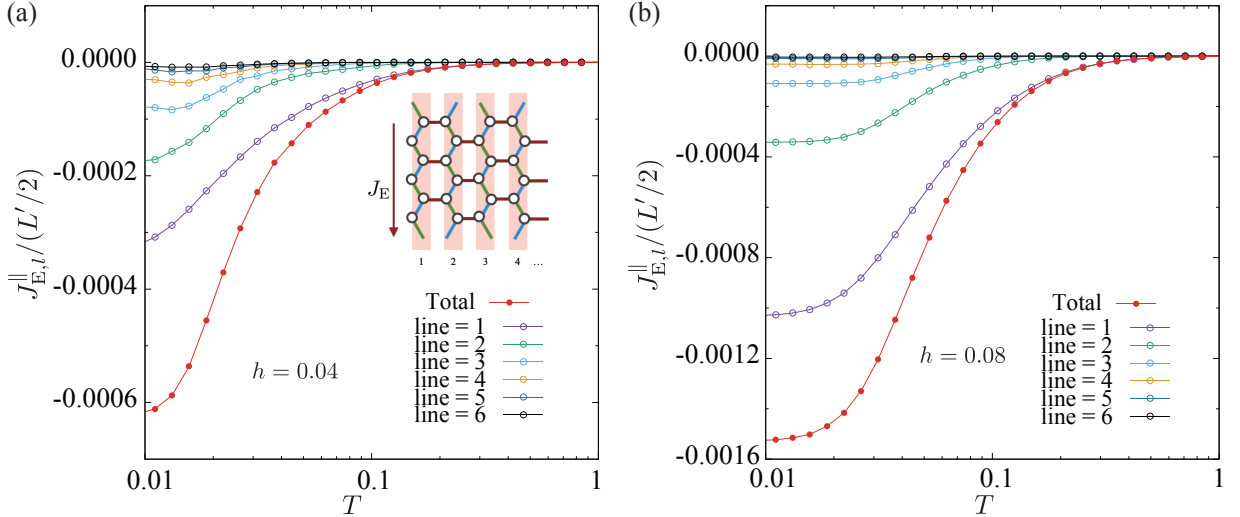


FIG. 4. Temperature dependence of the energy current of the ferromagnetic Kitaev model under (a)  $h = 0.04$  and (b)  $h = 0.08$ . In addition to the total energy current, the contribution from each line is shown.

temperatures, which is significantly reduced from  $W = 1$  in the ideal Kitaev QSL. As we show later, even at this high-magnetic region, the thermal Hall conductivity still remains large. We note that there is a phase transition between a chiral spin liquid and the paramagnetic phases around  $h_c \simeq 0.02$  [62, 63]. However, in the present calculations, we do not observe clear singularity indicating the phase transition due to finite size effects or because the calculation has not been carried out at sufficiently low temperatures to observe its signatures.

In Fig. 4, we show the total energy current defined in Eq. (9) for two representative magnetic fields,  $h = 0.04$  and  $h = 0.08$ . We find that the energy currents monotonically decrease as a function of the temperature from  $J_E^{\parallel} = 0$  in the high-temperature limit. This behavior indicates that  $\kappa_{xy} = dJ_E^{\parallel}/dT$  is positive and consistent with the expectation of the zero temperature limit.

To examine the spatial distribution of the energy current, we plot the position-dependent energy currents in Fig. 4. By changing its position from the edge side ( $l = 1$ ) to the center ( $l = 6$ ), the amplitude of the energy current decreases. This result demonstrates that the edge current mainly contributes to the thermal Hall conductivity. The dominant contribution of the edge current indicates that the nonzero thermal Hall conductivity reflects the topological nature of the excitation structure. We also realize that the decay of the current amplitude toward the center becomes faster when we increase the magnetic field. This behavior might be explained by the increase in the excitation gap of quasiparticles carrying the energies. Since the contributions from the center region are sufficiently small, the system size that we employ is sufficiently large to capture the essence of the thermal Hall conductivity.

Here, we discuss the temperature dependence of the

thermal Hall conductivity by evaluating the numerical derivative of  $J_E^{\parallel}$ , i.e.,  $\kappa_{xy} = d\langle J_E^{\parallel} \rangle/dT$ . Obtained  $\kappa_{xy}/T$  are shown in Fig. 3 (d). Except for small magnetic fields, we see clear peak structure in Fig. 3 (d): for example, the peak appears around  $T = 0.02$  for  $h = 0.05$ . The peak temperatures move to a higher temperature side with increasing  $h$ . They appear to be correlated with the low-temperature peaks of the specific heat. Thus, this result indicates that  $\kappa_{xy}/T$  around this temperature region is governed by the local flux degrees of freedom.ここまで言い切れるのか不安です Interestingly,  $\kappa_{xy}/T$  becomes much larger than the half-quantized value (shown by the broken line) at intermediate temperatures. Such an overshooting behavior was not observed in the previous numerical calculations, which treats the magnetic fields as the effective three-body interactions [26]. We note that in the low-temperature limit, we do not find any clear signature of the convergence of  $\kappa_{xy}/T$  to the half-quantized value even when the magnetic field is sufficiently small. As we discussed above, for  $h \lesssim 0.04$ , the bond dimension  $D = 500$  is not sufficient to obtain reliable results below  $T \sim 0.01$ . Moreover, due to the finite-size effects, even for the sufficiently small  $h$ , the expected chiral edge mode might have a finite gap. This finite-size gap might make  $\kappa_{xy}/T$  zero in the low temperature limit. Thus, in the present calculations, we do not deeply discuss the behavior of  $\kappa_{xy}/T$  at low magnetic field ( $h \lesssim 0.02$ ) and low-temperature region ( $T \lesssim 0.05$ ), where the effects of the finite bond dimensions and finite sizes become serious.

To gain more insights on the thermal Hall conductivity, we separate it into the two parts  $\kappa_{xy}^{(L)}$  and  $\kappa_{xy}^{(M)}$ , which are contributions from the three-body and the two-body correlations defined in Eqs. (7) and (8), respectively. Figures 3(e) and (f) shows the temperature de-

pendence of  $\kappa_{xy}^{(L)}$  and  $\kappa_{xy}^{(M)}$ . We find that the three-body part  $\kappa_{xy}^{(L)}/T$  dominantly contribute to the total  $\kappa_{xy}/T$  for all magnetic fields. In contrast to this, the contributions from tow-body part  $\kappa_{xy}^{(M)}/T$  are an order of magnitude smaller than those from the three-body part. Moreover, the peak of  $\kappa_{xy}^{(L)}/T$  develops with increasing  $h$  up to  $h = 0.04$  and shifts to the high-temperature side as shown in Fig. 3(e).” Moreorver...”の文、元の修正では、 $\kappa_{xy}/T$ と書いていましたが、それだと意味が通らないので、 $L$  termのことだと推測して修正しました。それでも、変な気がするので、この文章自体を削除したい気がしました。

Here, we discuss the origin of thermal Hall effect. Since the three-body part terms include the effective magnetic field obtained from the third-order perturbations for  $\mathbf{h}$ ,  $\kappa_{xy}^{(L)}$  is expected be related to the topological Majorana gap in the emergent Majorana fermion system. In contrast to the three-body part, the two-body part is linear with the magnetic field. This indicates that  $\kappa_{xy}^{(M)}$  is caused by effects beyond noninteracting Majorana fermion picture, which may contain contributions from magnons. The low-field behavior is consistent with Majorana fermion picture where the topological property becomes rigid by an applied magnetic field, but it cannot be accounted for by the magnon picture where the absolute value of  $\kappa_{xy}/T$  should monotonically decrease by applying the magnetic field [64]. Our results suggest that Majorana-like excitations dominantly contribute to the thermal Hall effect via the three-body spin part  $\kappa_{xy}^{(L)}$ .

## 2. Field-angle dependence

In this section, we examine the the filed-angle dependence of physical quantities in the pure Kitaev model. Figure 5 shows the results for  $h = 0.04$  and  $h = 0.08$ . We find that the specific heat and the magnetization do not show significant change among different directions while the flux significantly decreases for  $[\bar{1}10]$  direction. This behavior might be related to the presence of low-energy fluctuations due to the gapless Majorana dispersion for  $[\bar{1}10]$  direction.

While thermodynamic quantities such as the specific heat and the magnetization is insensitive for the field direction, the thermal Hall conductivity shows strong field-angle dependence. We examine the field-angle dependence in  $\kappa_{xy}$ . If the Majorana fermions or topological magnons govern the thermal Hall conductivity,  $\kappa_{xy}$  should change its sign according to the directions of the magnetic field since the sign of the Chern number depends on the directions of magnetic fields. For example, it is expected that  $\kappa_{xy}$  becomes positive (negative) for  $[111]$  magnetic field, while  $\kappa_{xy}$  becomes negative (positive) for  $[112]$  magnetic field in the wide temperature region for the case of Majorana fermion (topological magnon) picture [64–66]. We will examine whether

$\kappa_{xy}/T$  satisfies these direction dependencies in the original spin representation.

Figures. 5(d-f) show temperature dependence of  $\kappa_{xy}/T$  for three magnetic-field directions at  $h = 0.04$  and  $h = 0.08$ . By changing the direction of the magnetic field from  $\mathbf{h} \parallel [111]$  to  $\mathbf{h} \parallel [112]$ ,  $\kappa_{xy}/T$  changes the sign from positive to negative. We also find that the three-body part  $\kappa_{xy}^{(L)}$  is dominant and govern the sign of the total  $\kappa_{xy}$  in both cases. In  $\mathbf{h} \parallel [1\bar{1}\bar{2}]$  case,  $\kappa_{xy}^{(M)}$  becomes negative but small for  $h = 0.04$ . These results suggest that the Majorana fermion picture is rather plausible for explaining field-angle dependence of the thermal Hall effect in addition to the field-intensity dependence.

In  $\mathbf{h} \parallel [\bar{1}10]$  case, we find the  $\kappa_{xy}$  is nearly zero for all temperature region. From the symmetry of the Hamiltonian, we can explicitly show that  $\kappa_{xy}$  becomes zero. The Hamiltonian is invariant under the following two operations simultaneously: The  $C_2$  rotation along the  $[\bar{1}10]$  axis in the spin space transferring  $(S^x, S^y, S^z)$  to  $(-S^y, -S^x, -S^z)$  and the rotation of the honeycomb plane along the  $z$  bond in the real space, which exchanges the  $x$  and  $y$  bonds. However, the rotation of the honeycomb plane inverts the component of the position vector  $\mathbf{r}$  along the zigzag edge, and thereby, the thermal current along the zigzag edge should be zero. Note that the above argument is applicable in the presence of the  $\Gamma$  and  $\Gamma'$  interactions.

The change of  $\kappa_{xy}$  depending on the field angles is probably explained both by the Majorana fermions [1] and the topological magnons [64–66]. Although the sign of  $\kappa_{xy}$  in the case of topological magnon is different from our calculations, in principle, it is difficult to separate two contributions in thermal Hall conductivity at a finite temperature.

## B. Effect of non-Kitaev interactions

In this subsection, we investigate the effect of the symmetric off-diagonal interactions,  $\Gamma$  and  $\Gamma'$  terms, on the thermal Hall conductivity. From the magnetic field dependence in the Kitaev model, the elementary excitations appears to be dominated by Majorana fermions rather than magnons, particularly for the weak magnetic-field limit. As we denoted in Introduction, from the perturbative theory in the Majorana fermio representation, it is shown that the negative  $\Gamma'$  enhances the Majorana gap [67]. Hence, it is expected that the thermal Hall conductivity is enhanced by the negative  $\Gamma'$ . In contrast to  $\Gamma'$ , the perturbative expansion with respect to  $\Gamma$  is not straightforward, and it is not at all clear how  $\Gamma$  affects the thermal Hall conductivity. Here, we examine the impacts of  $\Gamma'$  and  $\Gamma$  interactions in the original spin representation without assuming the Majorana excitations.

### 1. Symmetric off-diagonal interaction $\Gamma'$

First, we consider the effect of  $\Gamma'$  interaction to  $\kappa_{xy}/T$  using two representative magnetic fields in the [111] direction,  $h = 0.04$  and  $h = 0.08$ . In Figs. 6(a)-(c), we show several physical quantities for  $-0.02 \leq \Gamma' \leq 0.02$ . We set, here,  $\Gamma = 0$  to only examine the effects of  $\Gamma'$  term. We find that  $\Gamma'$  does not significantly change the overall temperature dependence of the specific heat, although low-temperature peaks slightly move to higher (lower) temperatures for negative (positive)  $\Gamma'$ . We also find that the magnetization monotonically increase (decrease) for the negative (positive)  $\Gamma'$ . This  $\Gamma'$  dependence of the magnetization is consistent with the result of the perturbation theory [これは要確認]. In contrast to the magnetization, the flux does not show considerable changes as a function of  $\Gamma'$ .

Figs. 6(d)-(f) show temperature dependence of  $\kappa_{xy}/T$  with the same  $\Gamma'$ 's. Although the effects to the bulk physical quantities are small as we showed above,  $\Gamma'$  largely changes  $\kappa_{xy}/T$ ; when we decrease  $\Gamma'$  from  $\Gamma' = 0.02$ , the peak of  $\kappa_{xy}/T$  moves to higher temperature with increasing its height. In particular, for the negative (positive)  $\Gamma'$ , the increase of its absolute value leads to the enhancement (suppression) of  $\kappa_{xy}/T$ . Such sign-dependent changes of  $\kappa_{xy}$  are consistent with the perturbation theory [18].

We also find that  $\Gamma'$  monotonically decreases both the three-body part and the two-body part of  $\kappa_{xy}$ ; With increasing  $\Gamma'$  from  $\Gamma' = -0.02$ ,  $\kappa_x^{(L)}$  is suppressed and its peak shifts to the low-temperature side [Fig. 6(e)], similar to the total thermal Hall conductivity [Fig. 6(d)]. On the other hand,  $\kappa_x^{(L)}$  exhibits the sign change from the positive to negative [Fig. 6(f)]. For  $\Gamma' \geq 0.01$ , the two-body part  $\kappa_x^{(M)}$  becomes negative and there is a competition between the positive  $\kappa_x^{(L)}$  and the negative  $\kappa_x^{(M)}$ . As a result, in  $\Gamma' = 0.02$  and  $h = 0.04$ , the total  $\kappa_{xy}/T$  becomes negative around  $T = 0.04$ , although its absolute value is small. このnegativeになる記述は必要? → 残したいです

### 2. Symmetric off-diagonal interaction $\Gamma$

Next, we investigate effects of  $\Gamma$  term on  $\kappa_{xy}/T$  under a magnetic field parallel to the [111] direction. Again we consider two representative magnetic fields,  $h = 0.04$  and  $h = 0.08$ . In Figs. 8(a)-(c), we show the temperature dependence of the specific heat, the magnetization, and the flux for  $-0.02 \leq \Gamma \leq 0.02$ . Although the amplitudes of  $\Gamma$  are relatively small, we find that the low-temperature peaks of the specific heat show significant change. For negative  $\Gamma$ , the peak moves to a higher temperature, and its height is enhanced. Similarly, the magnetization increases for negative  $\Gamma$ . For positive  $\Gamma$ , we observe the opposite effects. We can also see sign-dependent changes in the flux around intermediate temperature re-

gion  $T \sim 0.03$ , although it is not so significant.

As shown in Figs. 8(d)-(f), we find that the  $\Gamma$  term can change the thermal Hall conductivity significantly. Negative  $\Gamma$  suppresses  $\kappa_{xy}/T$  both for  $h = 0.04$  and  $h = 0.08$ . In the case of positive  $\Gamma$ , we see different behaviors between  $h = 0.04$  and  $h = 0.08$ . For  $h = 0.04$ , positive  $\Gamma$  largely suppresses  $\kappa_{xy}/T$ , and it becomes even negative for  $\Gamma = 0.02$ . In contrast to  $h = 0.04$ , we see that positive  $\Gamma$  enhances  $\kappa_{xy}/T$ . Such huge changes in  $\kappa_{xy}/T$  by small  $\Gamma$  seem to be different from the result of perturbation theory; it shows the contributions from  $\Gamma$  appear as the third order [19].

This magnetic field-dependent behavior might be related to the large  $\kappa_{xy}^{(M)}/T$  for positive  $\Gamma$ . For  $\Gamma \leq 0$ ,  $\kappa_{xy}^L$  dominate the total  $\kappa_{xy}/T$ . However, for  $\Gamma = 0.01$  and  $0.02$ , the low-temperature value of  $\kappa_{xy}^{(M)}/T$  largely increases as shown in Fig. 8(f). This abrupt change may recall the presence of a phase transition from the Kitaev QSL to another phase such as a spin nematic state, which is suggested by using the infinite tensor network calculation at zero temperature [39].

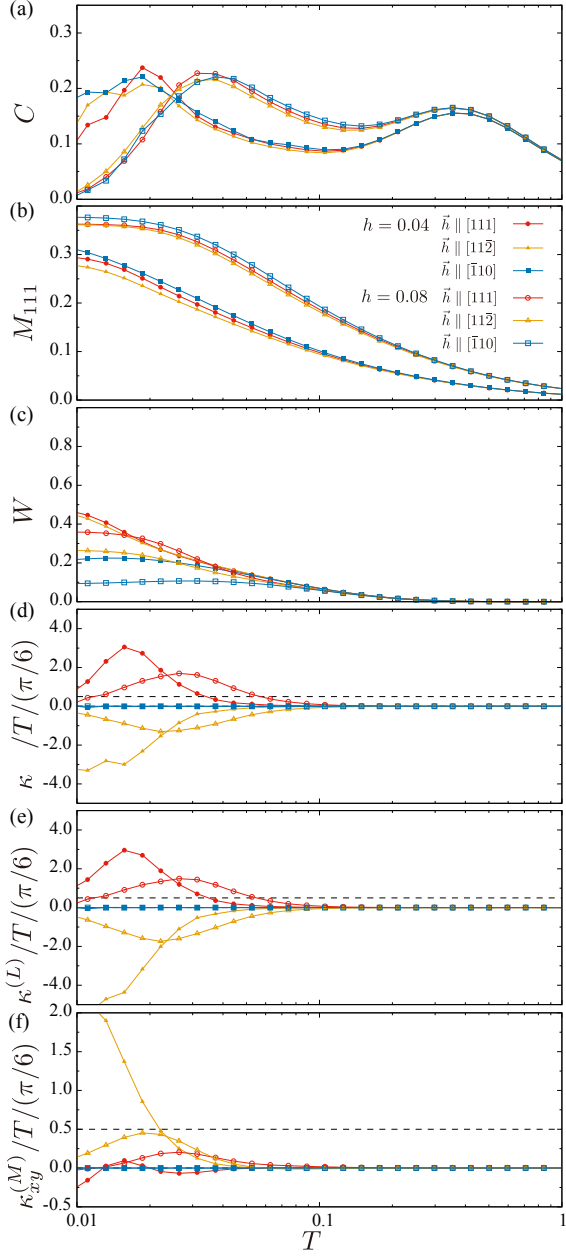


FIG. 5. Temperature dependence of (a) the specific heat (b) the magnetic moment (c) the flux, and (d)  $\kappa_{xy}/T$  of the ferromagnetic Kitaev model under magnetic fields parallel to [111], [112], and [110] with  $|h| = 0.04$  and  $|h| = 0.08$ . (e),(f) Contributions from the three-body ( $L$ ) and the two-body ( $M$ ) terms to  $\kappa_{xy}/T$ , respectively. Two horizontal dashed lines indicate  $\kappa_{xy}/T = 0$  and the half-quantized value. [b軸で低温での比熱のデータが切れている理由は何かあるでしょうか。b軸でエントロピーが残りやすいような振る舞いがあれば実験と関係するかもしれません。]→[大久保さんが追計算してくださいました]

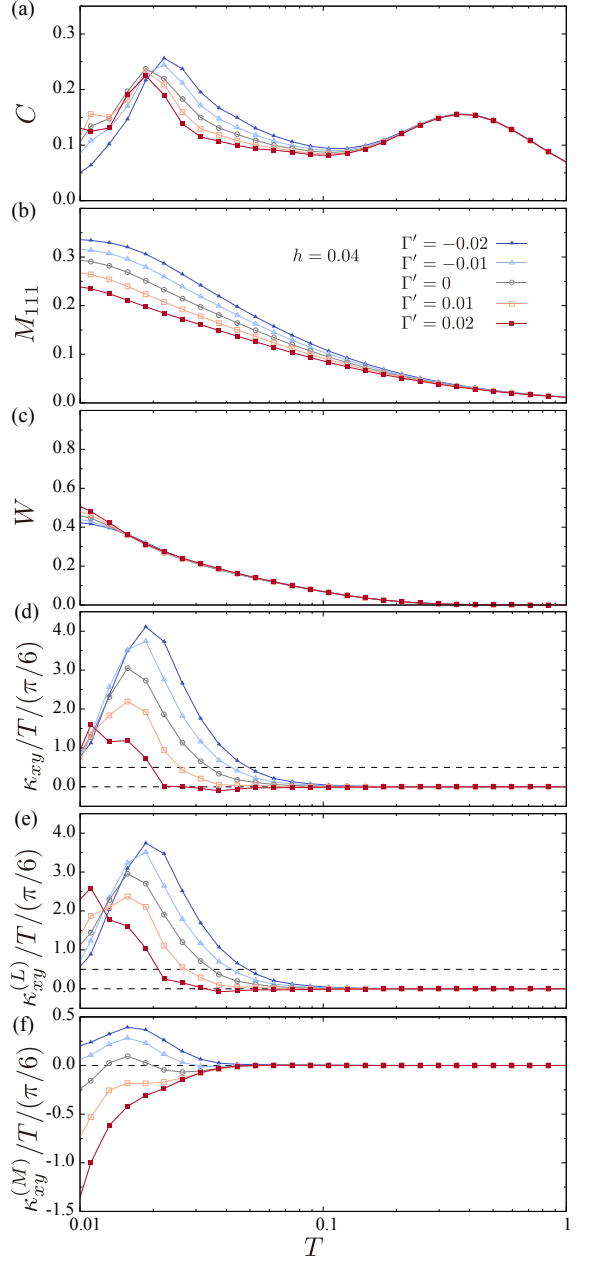


FIG. 6. Temperature dependence of (a) the specific heat (b) the magnetic moment, (c) the flux (d) the total thermal Hall conductivity  $\kappa_{xy}/T$ , (e) the three-body part of the thermal Hall conductivity  $\kappa_{xy}^L/T$ , and (f) the two-body part of the thermal Hall conductivity  $\kappa_{xy}^M/T$  of the **extended Kitaev model with  $\Gamma = 0$  and varying  $\Gamma'$**  under a magnetic field parallel to [111] direction. The amplitude of the magnetic field is  $|h| = 0.04$ . [もう少し縦幅が狭い方がよい?]→対応しました

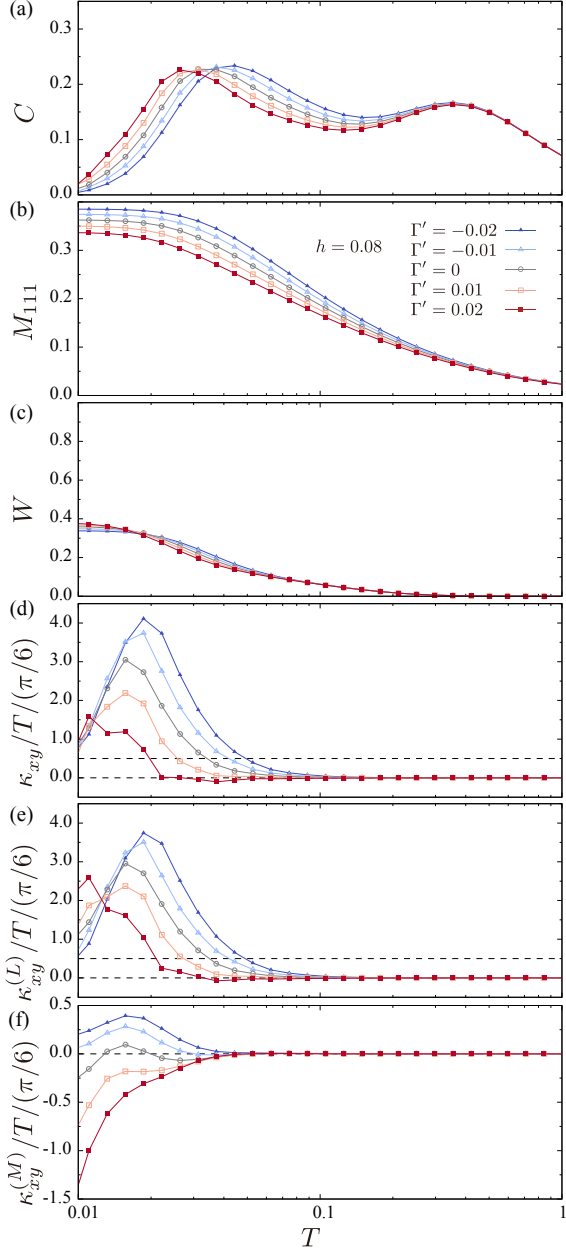


FIG. 7. Corresponding plots to Fig. 6 for the extended Kitaev model with  $\Gamma = 0$ ,  $h = 0.08$  and varying  $\Gamma'$ . [もう少し縦幅が狭い方がよい?]→対応しました

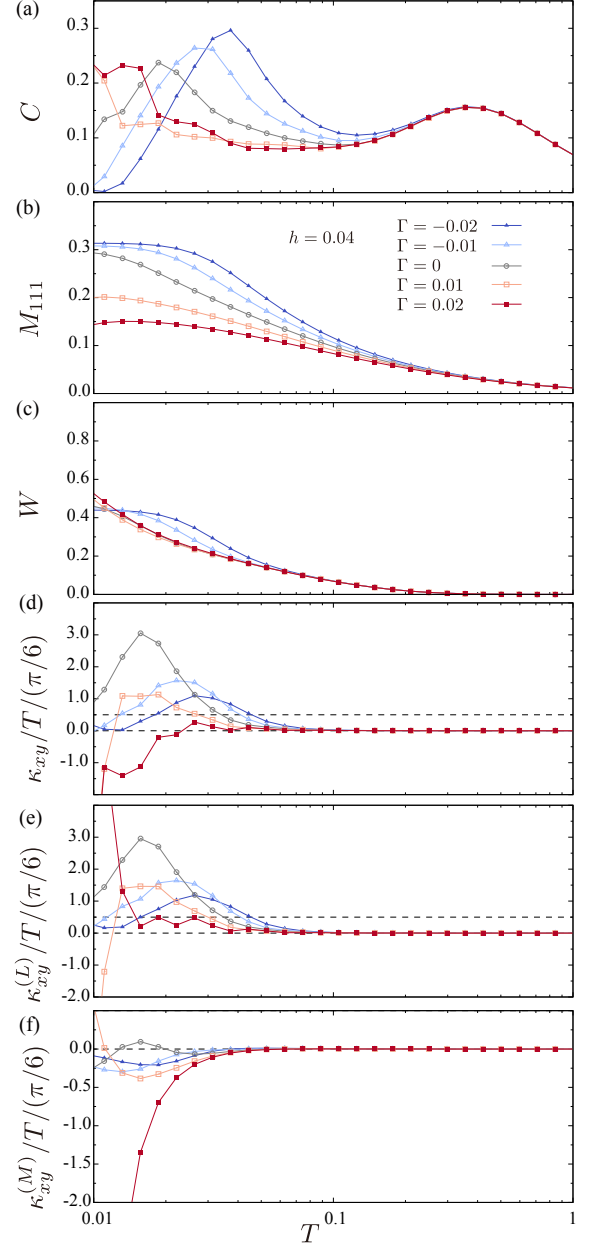


FIG. 8. Corresponding plots to Fig. 6 for the extended Kitaev model with  $\Gamma' = 0$ ,  $h = 0.04$  and varying  $\Gamma$ . [もう少し縦幅が狭い方がよい?]→対応しました

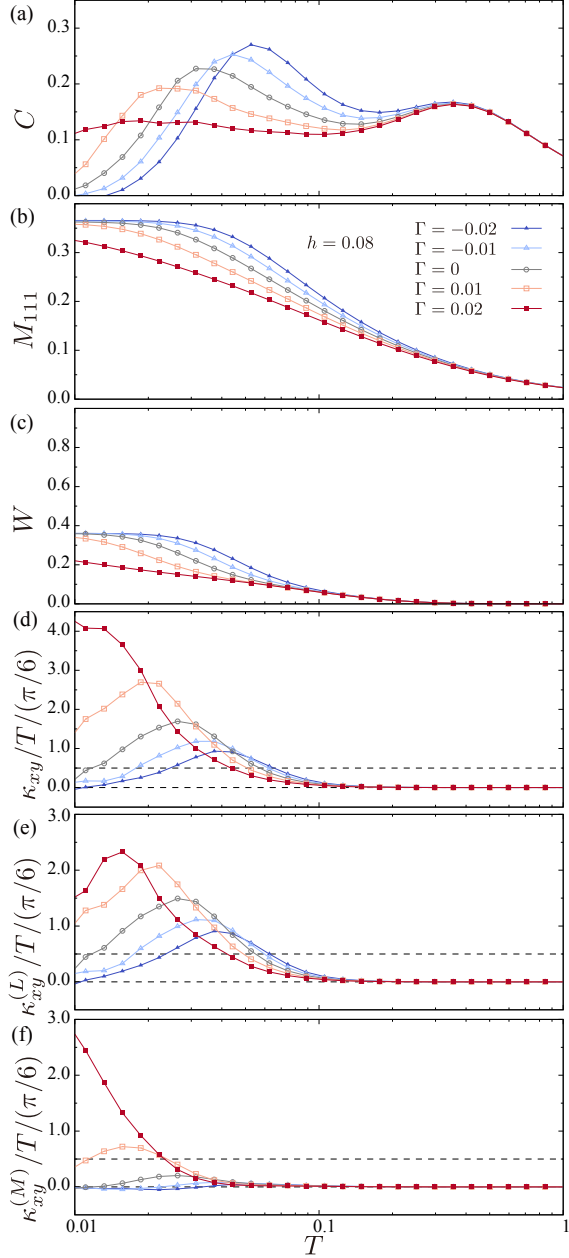


FIG. 9. Corresponding plots to Fig. 6 for the extended Kitaev model with  $\Gamma' = 0$ ,  $h = 0.08$  and varying  $\Gamma$ . [もう少し縦幅が狭い方がよい?] → 対応しました

### C. Classical limit

In this section, we show the results obtained by applying the classical approximation for Eq. (2) to compare those for the quantum spin model shown above. First, we focus on the pure Kitaev model with  $\Gamma = \Gamma' = 0$ . Figure 10(a) shows the temperature dependence of the specific heat of the classical Kitaev model at several magnetic fields along the [111] direction. In the absence of the magnetic field, the previous studies clarified that the specific heat monotonically increases with decreasing temperature and approaches  $3/4$  in the zero temperature limit [68, 69]. This value originates from the zero modes intrinsic to the pure Kitaev model without a magnetic field, and the quartic order of the spin fluctuations contributes to the specific heat at  $T \rightarrow 0$ . Once the magnetic field is introduced, it lifts the zero modes, and thereby, the zero- $T$  limit of the specific heat takes the conventional value, i.e., 1, owing to the presence of the two continuous variables  $(\theta, \phi)$  at each site. We find that it shows **shoulder structure** at the temperature corresponding to the energy scale of  $h$  in the presence of the magnetic field despite the monotonic change at  $h = 0$ . In this temperature scale, the magnetization **monotonically increases as a function of the magnetic field**, as shown in Fig. 10(b).

Figure 10(c) shows the thermal Hall conductivity as a function of temperature. When the magnetic field is not applied, this is always zero. By introducing the magnetic field,  $\kappa_{xy}$  becomes nonzero and positive, which is consistent with the results for the quantum system. Moreover, the temperature scale for developing the thermal Hall conductivity is much smaller than that for the magnetization. The distinctly different temperature scales appear to be similar to those in the quantum system [see Fig. 3] although the double-peak structure of the specific heat is not observed in the classical system. In the classical result,  $\kappa_{xy}$  shows a monotonic increase with decreasing temperature. On the other hand, in the quantum system,  $\kappa^{xy}/T$  takes a peak around the temperature at which the specific heat exhibits the low- $T$  peak, as shown in Fig. 3(e). The difference is considered to originate from an artifact in the classical system, where the macroscopic degeneracy is present in the low-energy region. **The degeneracy also causes the nonzero specific heat at zero temperature. Thus, the quantization of  $\kappa^{xy}/T$  does not occur in the classical system.** Figures 10(d) and 10(e) present the three-body and two-body contributions of the thermal current to the thermal Hall conductivity, respectively. The two-body contributions  $\kappa_{xy}^{(M)}$  is much smaller than the three-body one  $\kappa_{xy}^{(L)}$ , indicating that the thermal Hall effect is dominated by the three-body terms of the thermal current at the edges. **This result is consistent with the quantum system, but the classical approximation appears not to reproduce small negative values of  $\kappa_{xy}^{(M)}$  in weak magnetic fields as shown in Fig. 3(f).** The difference suggests that the negative  $\kappa_{xy}^{(M)}$  may be induced by quantum effects.

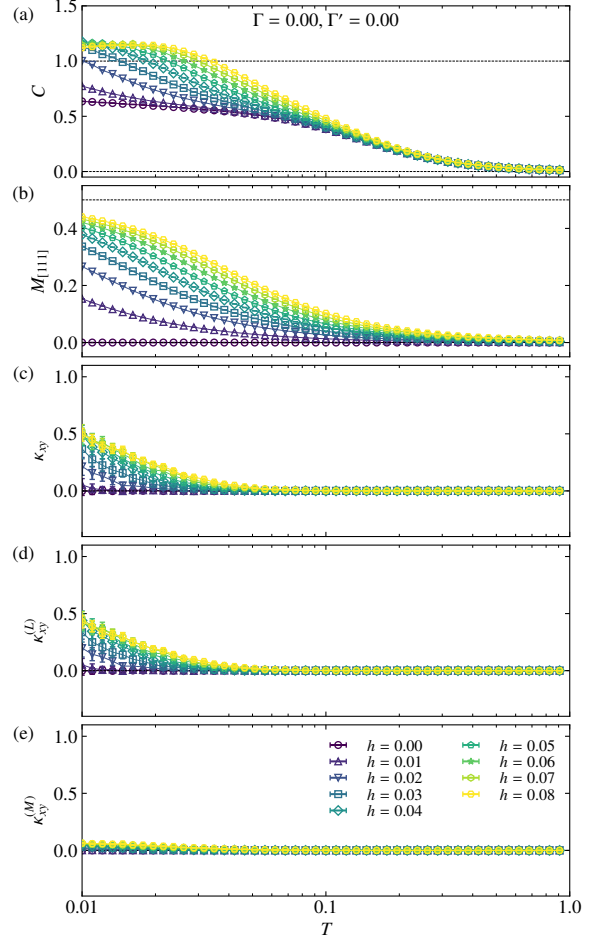


FIG. 10. Temperature dependence of (a) the specific heat, (b) the total magnetization, and (c) the thermal Hall conductivity  $\kappa_{xy}$  for several magnetic fields along the [111] direction in the classical Kitaev model. (d),(e) Temperature dependence of the two components, ( $L$ ) and ( $M$ ), of the thermal Hall conductivity.

Next, we discuss the field-angle dependence in the pure Kitaev model. We consider the three field directions  $[11\bar{2}]$ ,  $[\bar{1}10]$ , and  $[111]$ , which are perpendicular to each other. Figures 11(a) and 11(b) show the temperature dependence of the specific heat and magnetization along the corresponding field direction. These indicate that the field direction hardly changes the specific heat and magnetization, which is also observed in the quantum system (see Fig. 5).

**In contrast to these bulk quantities**, the thermal Hall conductivity strongly depends on the direction of the applied magnetic field. As shown in Figure 11(c),  $\kappa_{xy}$  is negative and decreases with decreasing temperature for  $\mathbf{h} \parallel [11\bar{2}]$  in contrast to the case with  $\mathbf{h} \parallel [111]$ . Moreover, the absolute value for the former is smaller than that for the latter. While **overall behaviors** are consistent with that in the quantum system, the peak structure in Fig. 5(d) is not seen in the classical case. Further-

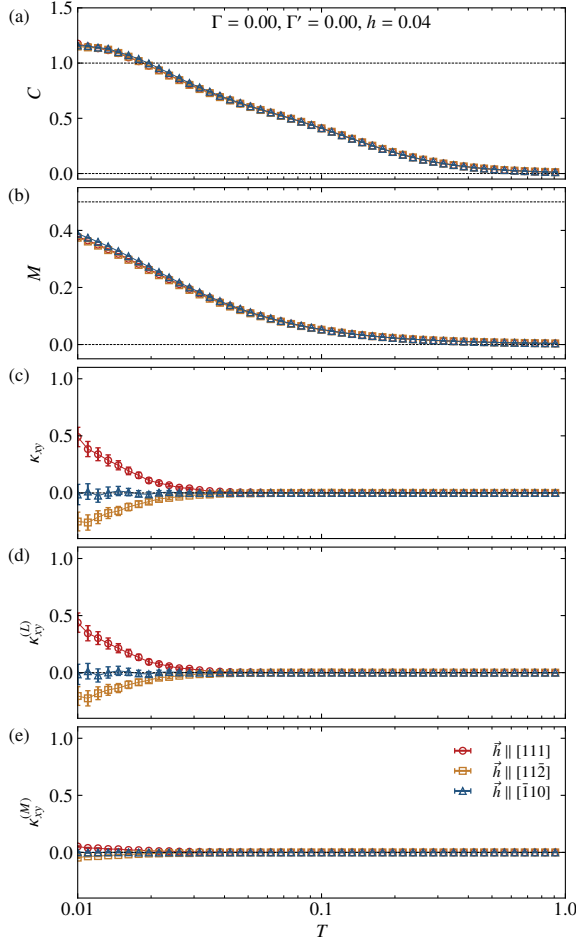


FIG. 11. Temperature dependence of (a) the specific heat, (b) the total magnetization, and (c) the thermal Hall conductivity  $\kappa_{xy}$  in the classical Kitaev model under the magnetic field parallel to [111], [11 $\bar{2}$ ], and  $[\bar{1}10]$  with  $h = 0.04$ . (d),(e) Temperature dependence of the two components, ( $L$ ) and ( $M$ ), of the thermal Hall conductivity.

more, a large enhancement of  $\kappa_{xy}^{(M)}$  at low temperatures for  $\vec{h} \parallel [11\bar{2}]$  presented in Fig. 5(f) is not reproduced in the classical system as shown in Fig. 11(e) despite the similarity for the temperature of  $\kappa_{xy}^{(L)}$  in the quantum and classical systems [Figs. 5(e) and 11(d)]. This result suggests that the three-body term can be understood in the classical picture, but quantum fluctuations beyond the classical approach substantially contribute to the two-body term. We also find that the thermal Hall conductivity is zero in the magnetic field applied along the  $[\bar{1}10]$  direction, which results in the symmetry of the Hamiltonian, as discussed before.

Here, we introduce the  $\Gamma'$  and  $\Gamma$  interactions in the Kitaev model. First, we examine the effect of the  $\Gamma'$  interaction on the Kitaev system. Figure 12 shows the temperature dependence of physical quantities for several values of  $\Gamma'$  in the Kitaev- $\Gamma'$  model without the  $\Gamma$  interaction. The positive  $\Gamma'$  suppresses the specific heat and magne-

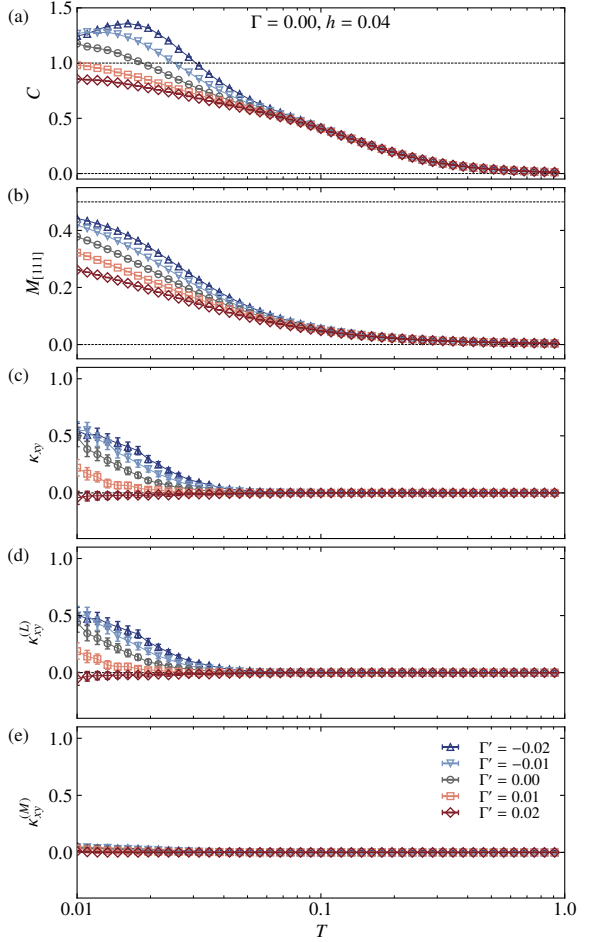


FIG. 12. Temperature dependence of (a) the specific heat, (b) the total magnetization, and (c) the thermal Hall conductivity  $\kappa_{xy}$  in the classical Kitaev- $\Gamma'$  model under the magnetic field with  $h = 0.04$ . (d),(e) Temperature dependence of the two components, ( $L$ ) and ( $M$ ), of the thermal Hall conductivity.

tization while the negative  $\Gamma'$  enhances them. Moreover, we find a peak in the specific heat at  $\Gamma' = -0.02$  in Fig. 12, indicating its shift to the high-temperature side with decreasing  $\Gamma'$ . These tendencies are also seen in the quantum system, as shown in Figs. 6(a) and 6(b).

For the thermal transport, we find that the negative (positive)  $\Gamma'$  enhances (suppresses) the thermal Hall conductivity [Fig. 12(c)]. We note that  $\kappa_{xy}$  becomes negative at low temperatures for  $\Gamma' = 0.02$ . We also find that the three-body part dominantly contributes to the thermal Hall conductivity, as shown in Figs. 12(d) and 12(e). Thus, the overall tendency is consistent with that of the quantum systems. Furthermore, by examining the temperature dependence in detail, we find that results for the classical limit are well consistent with those for the intermediate temperature range ( $T \sim 0.05$ ) in the quantum system shown in Fig. 6(a). In the quantum systems around  $T = 0.05$ ,  $\kappa_{xy}$  monotonically decrease by increasing  $\Gamma'$  and it appears to be negative for  $\Gamma' = 0.02$ . More-

over, in this temperature range,  $\kappa_{xy}^{(M)}$  is much smaller than  $\kappa_{xy}^{(L)}$ , as shown in Figs. 6(e) and 6(f). These results indicate that  $\kappa_{xy}$  in the classical systems corresponds to that in the quantum systems at intermediate temperatures, where the effects of the quantum fluctuations are expected to be small.

Finally, we focus on the effect of the  $\Gamma$  term. Figure 13 shows the temperature dependence of physical quantities at several values of  $\Gamma$  with  $\Gamma' = 0$ . For the case of the negative  $\Gamma$ , the low- $T$  specific heat is enhanced with increasing the absolute value of  $\Gamma$  as shown in Fig. 13(a). On the other hand, the specific heat is suppressed by the introduction of the positive  $\Gamma$ . These tendencies are consistent with the results in the quantum system, while peak structure shown in Fig. 8(a) is not reproduced in the classical simulations. Figure 13(b) shows the temperature dependence of the magnetization at several  $\Gamma$ . The magnetization increases with decreasing  $\Gamma$ , which is also observed in the quantum result shown in Fig. 8(b).

[あんまりこの段落の意図がわからないのですが、とりあえずおいておきます] [K- $\Gamma$ 模型の結果が量子系と合わないことの言い訳をしたかったので、K- $\Gamma$ 模型ではK- $\Gamma'$ 模型より量子効果が効きやすいことを入れてみました。] Meanwhile, from the comparisons of the effects of  $\Gamma'$  and  $\Gamma$  terms, we also find the behavior that is inconsistent with that in the quantum system. For the classical simulations, the specific heat and magnetization appear to be sensitive to  $\Gamma'$  rather than  $\Gamma$ , which is opposite to results in the quantum system (Figs. 8 and 6). This contrasting behavior suggests that the  $\Gamma'$  interaction stabilizes spin states with weak quantum fluctuations, but quantum effects play important roles in the Kitaev- $\Gamma$  model. Indeed, it has been pointed out that the  $\Gamma$  interaction does not destroy a QSL state [36, 70], whereas the introduction of  $\Gamma'$  shrinks the region of the QSL phase [45, 47].

While  $\Gamma$  dependence of the specific heat and the magnetization is consistent with that in the quantum system, the low-temperature behavior of the thermal Hall conductivity [Fig. 13(c)] is significantly different from that in the quantum system shown in Fig. 8. The characteristic feature of the results for the quantum system is the substantial enhancement of both  $\kappa_{xy}^{(L)}$  and  $\kappa_{xy}^{(M)}$ , which are almost canceled out in the total thermal Hall conductivity  $\kappa_{xy}$ . This is not reproduced in the classical system, suggesting that it is yielded by quantum fluctuations. Nevertheless, in the intermediate temperature region around  $T = 0.05$  in Fig. 8, we again find that the  $\Gamma$  and temperature dependencies are similar to the low-temperature behavior in the classical system shown in Figs. 13(c)–13(e). These results imply that the behavior in the intermediate temperature region of the quantum system is understood by the classical regime because the effects of the quantum fluctuations are not large.

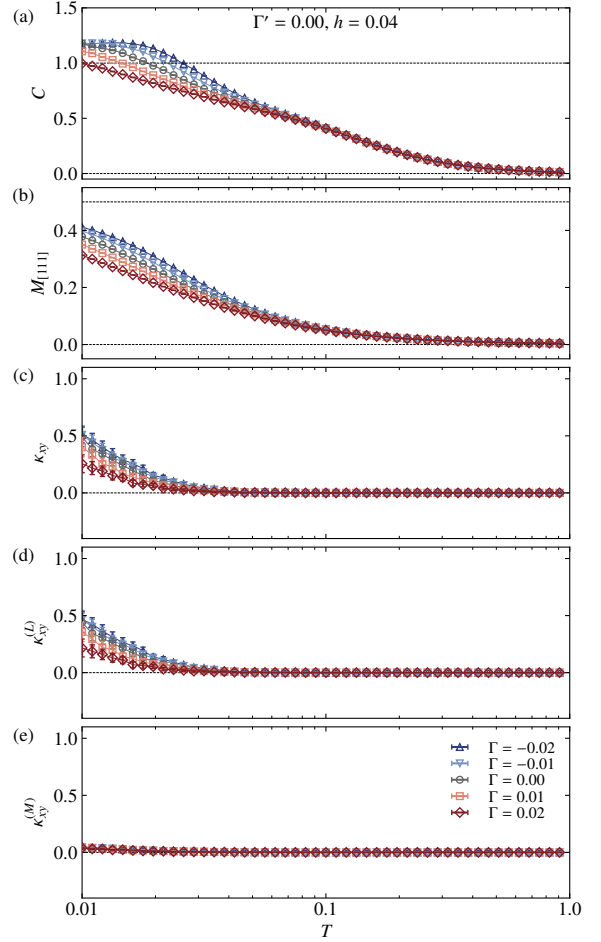


FIG. 13. Temperature dependence of (a) the specific heat, (b) the total magnetization, and (c) the thermal Hall conductivity  $\kappa_{xy}$  in the classical Kitaev- $\Gamma$  model under the magnetic field with  $h = 0.04$ . (d),(e) Temperature dependence of the two components, ( $L$ ) and ( $M$ ), of the thermal Hall conductivity.

#### D. Summary of temperature field dependence

In this section, we summarize the temperature and the magnetization field dependence of  $\kappa_{xy}$  in both quantum and classical systems. In Figs. 14, we show the two-dimensional color plots of  $\kappa_{xy}/T$  varying the temperature and the magnetic field for various  $\Gamma$  and  $\Gamma'$ , respectively. Firstly, we can see that peaks in  $\kappa_{xy}/T$  appear in the  $h$ - $T$  plane. We note that the peak heights overshoot the half-quantized value. By introducing a weak  $\Gamma'$  interaction to the pure Kitaev model, the strong enhancements of  $\kappa_{xy}/T$  are observed for negative  $\Gamma'$ , while positive  $\Gamma'$  suppresses  $\kappa_{xy}/T$ . The negative  $\kappa_{xy}/T$  observed for smaller  $h$  and lower temperature are probably due to the small  $D$  effects. In the case of  $\Gamma$ , we can see that negative  $\Gamma$  suppresses  $\kappa_{xy}/T$ , while positive  $\Gamma$  can largely enhance it for high magnetic fields. In addition, positive  $\Gamma$  makes  $\kappa_{xy}/T$  negative at small magnetic fields. By comparing  $\Gamma = 0.01$  and  $0.02$ , we realize that the region of negative  $\kappa_{xy}/T$  moves to higher magnetic fields. This trend might be related to possible quantum phase transition as discussed above.

In Fig. 15, we show the color plot of  $\kappa_{xy}$  in the  $h$ - $T$  plane of the classical model. We can see that  $\Gamma$  term do not affects the overall behavior of  $\kappa_{xy}$ , while negative (positive)  $\Gamma'$  enhance (diminish)  $\kappa_{xy}$ . The insensitivity to the  $\Gamma$  term is in contrast to the results for quantum systems. Thus, the effects of  $\Gamma$  term are governed by the quantum effects while those of  $\Gamma'$  can be captured by the classical model.

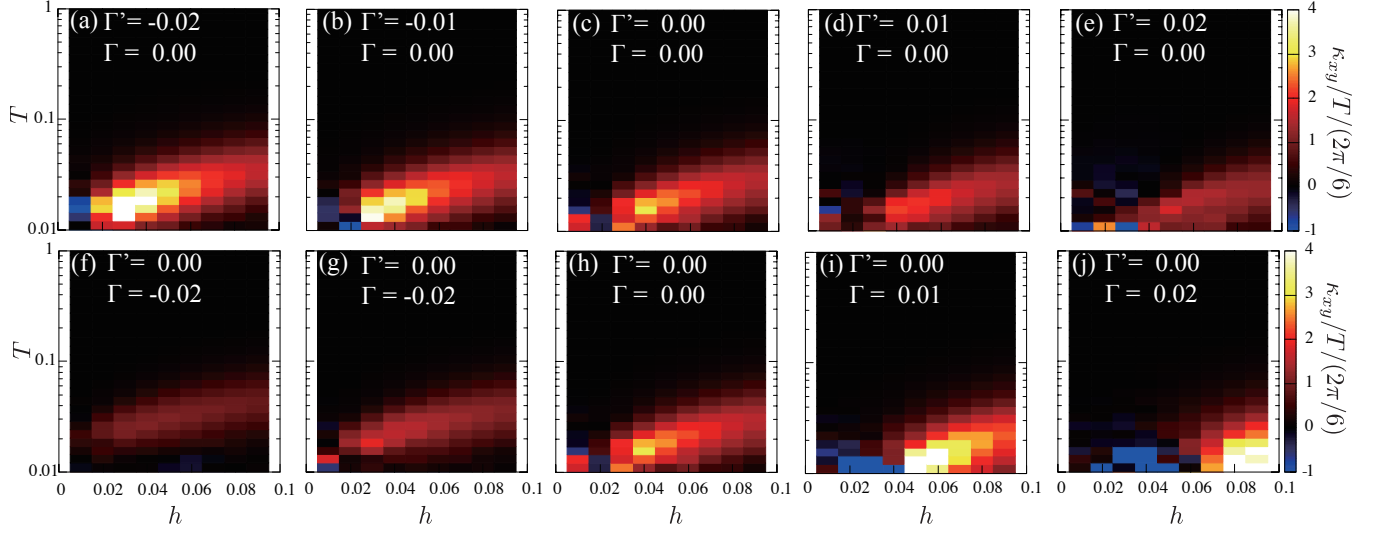


FIG. 14. (a)-(e) Color maps of  $\kappa_{xy}/T$  for ferromagnetic Kitaev model with  $\Gamma = 0, \pm 0.01, \pm 0.02$  with various magnetic fields and temperatures. (f)-(j) Color maps of  $\kappa_{xy}/T$  for ferromagnetic Kitaev model with  $\Gamma' = 0, \pm 0.01, \pm 0.02$  with various magnetic fields and temperatures.

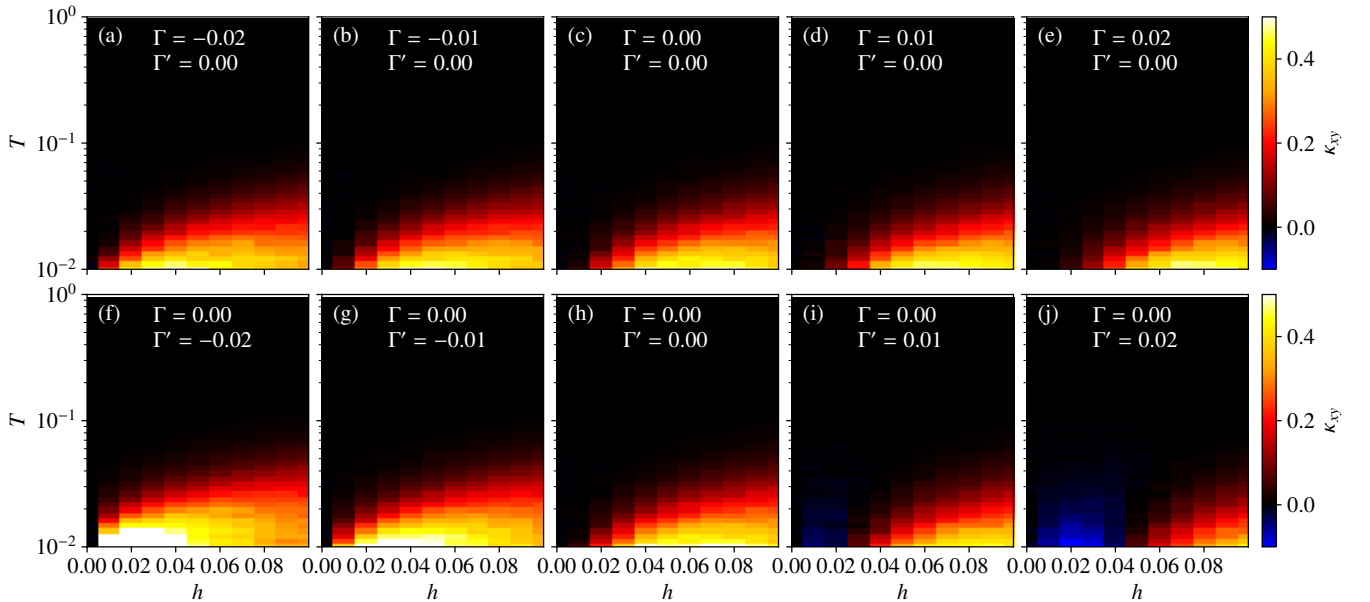


FIG. 15. Corresponding plots to Fig. 14 for the classical model.

## V. SUMMARY

In this study, we show a systematic analysis of thermal Hall conductivity in the extended Kitaev model at finite temperatures using the tensor-network representation of the density matrix. This method enables us to perform a highly-accurate analysis of thermal Hall conductivity beyond the conventional perturbation theory. The significant finding is that the thermal Hall conductivity largely exceeds the half-quantized value. This result indicates that the large thermal Hall conductivity observed in  $\alpha$ -RuCl<sub>3</sub> experiments can be explained by the physics of the Kitaev model. We show that the field-angle dependence of the thermal Hall conductivity is consistent with that obtained by the Majorana picture even under a high magnetic field.

We also show that the thermal Hall conductivity is significantly affected by the  $\Gamma$  and  $\Gamma'$  terms even when their amplitudes are two orders of magnitude smaller than the Kitaev interaction. In particular, in the case of the negative  $\Gamma'$  and the positive  $\Gamma$ , the thermal Hall conductivity is enhanced. However, the origins of the enhancement are quite different. For the negative  $\Gamma'$ , we find that the three-body term  $\kappa_{xy}^{(L)}$  is the main contributor to the enhancement, which is consistent with the scenario that the Majorana gap is increased by the negative  $\Gamma'$  term [67]. In contrast to this, for the positive  $\Gamma$  case, the enhancement is governed by the two-body part  $\kappa_{xy}^{(M)}$ . This mechanism is not simply understood from the perturbation theory and may be related to the possible phase transitions induced by the  $\Gamma$  term. By comparing with the results from classical systems, we find that the main effect of the  $\Gamma'$  term can be captured in classical systems, whereas the effect of the  $\Gamma$  term cannot. In other words, the behaviors of the three-body part  $\kappa_{xy}^{(L)}$  can be reproduced by the classical model but  $\kappa_{xy}^{(M)}$  cannot. This result suggests that the  $\Gamma$  term has a larger quantum mechanical effect.

[実験との関連やtopological magnonとの関連の議論を追加する?]

## ACKNOWLEDGMENTS

We wish to thank Y. Kato and K. Fukui for fruitful discussions. TM was supported by Building of Consortia for the Development of Human Resources in Science and Technology, MEXT, Japan. This work was supported by Grant-in-Aid for Scientific Research Nos. 19H05825, 19K03742, 20H00122, and 23H03818 from the Ministry of Education, Culture, Sports, Science and Technology, Japan. It is also supported by JST CREST Grant No. JPMJCR18T2 and JST PRESTO Grant No. JP-MJPR19L5. This work was also supported by the National Natural Science Foundation of China (Grant No. 12150610462).

## Appendix A: Benchmark on tensor network method

In this section, we present several benchmark results for the XTRG method. Firstly, we show bond-dimension dependence of the several physical quantities of the pure Kitaev model on the  $(L, L') = (6, 6)$  cylinder in Fig. 16. We find that  $D$  dependence becomes larger for  $T \lesssim 0.05$  for the specific heat and the thermal Hall conductivity in  $h = 0.04$ . However, in  $D = 500$ , we can obtain clear peak structures in the specific heat and the thermal Hall conductivity and their values are not so deviated from those of  $D = 400$ . Thus, we consider that the  $D = 500$  is sufficiently large to discuss the thermal Hall conductivity for  $(L, L') = (6, 6)$ ,  $T \geq 0.01$ , and  $h \geq 0.04$ .

Next, for another system size  $(L, L') = (8, 4)$ , we examine the bond-dimension dependence of the physical quantities. As shown in Fig. 17, up to  $D = 400$ , we obtained almost converged data even for the specific heat and the thermal Hall conductivity at  $h = 0.04$ . Although the accuracy of the matrix product representation depends on the circumference, i.e., system sizes, we can obtain the almost converged results for  $D = 400$ . These results demonstrate that the XTRG method with sufficiently large  $D$  is a powerful tool for investigating finite-temperature properties of quantum spin systems.

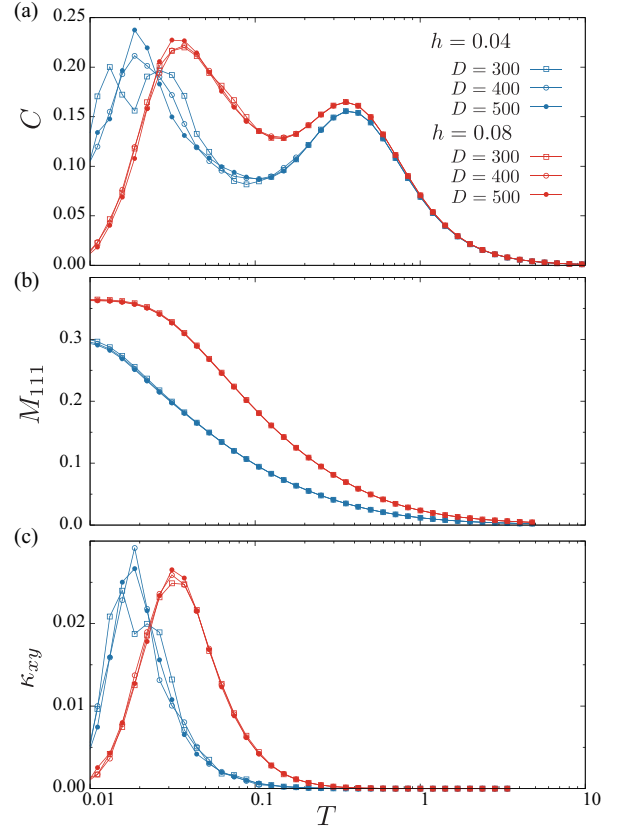


FIG. 16. Temperature dependence of (a) the specific heat (b) the magnetic moment, and (c) the thermal Hall conductivity of the ferromagnetic Kitaev model for the external magnetic field  $h = 0.04$  and  $h = 0.08$  parallel to [111] direction with different bond-dimensions  $D = 300, 400, 500$ . The lattice is  $(L, L') = (6, 6)$

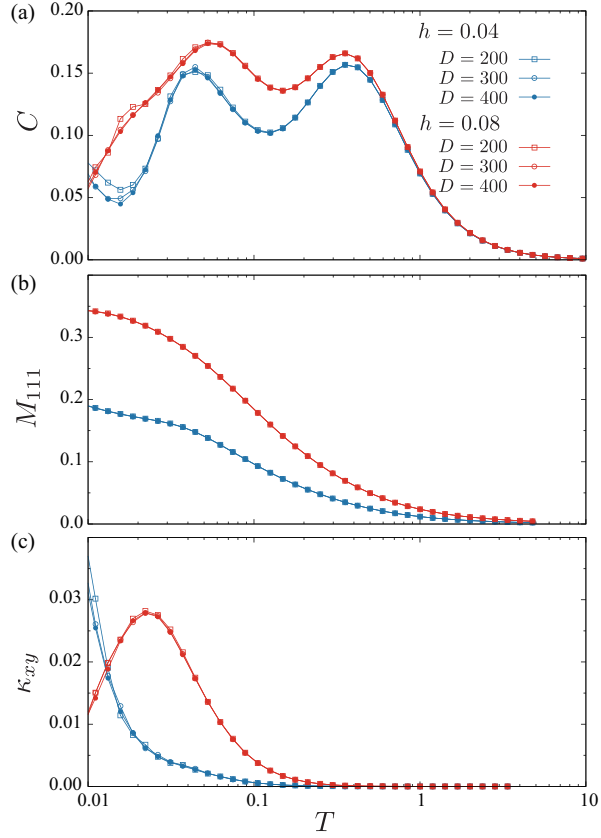


FIG. 17. Corresponding plot to Fig. 16 for  $(L, L') = (8, 4)$ .

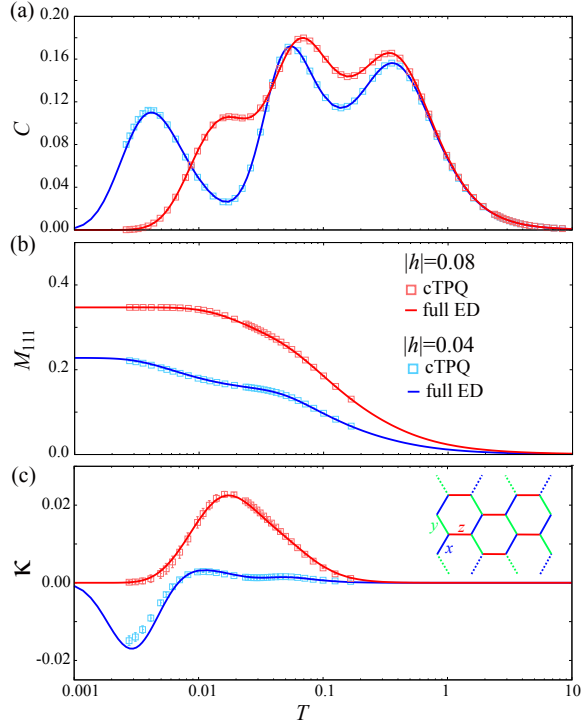


FIG. 18. Temperature dependence of (a) the specific heat, (b) the total magnetization, and (c) the thermal Hall conductivity  $\kappa$ . In the bootstrap sampling, we take 1000 independent initial states, and choose 1000 samples 500 times with replacement to evaluate the average values and the error vars.

## Appendix B: Benchmark on thermal pure quantum state

この節はそもそもいらない気がしますが...→とりあえず、情報はあっても良いと思ったので、残しています

We examine the accuracy of the cTPQ method in this section by comparing the results of the cTPQ method with the full diagonalization for a small  $(L, L') = (2, 4)$  cluster (the total system size is  $N_s = 16$ ). In the full exact diagonalization (full ED) method, we diagonalize Hamiltonian whose dimension is  $2^{16} = 65536$  using ScaLA-PACK [71]. Using obtained eigenvalues and eigenvectors, we calculate the temperature dependence of the physical quantities.

At  $h = 0.04$ , the specific heat  $C$  has three-peak structures in this geometry. These three structure may be the finite-size effects since it vanishes for larger system sizes. Even at  $h = 0.08$ , the hump in the specific heat still exists around  $T = 0.02$ . As shown in Fig. 18(a), the

cTPQ method reproduces the temperature dependence of the specific heat for  $h = 0.04$  and  $h = 0.08$  including the multiple peak structures. Fig. 18(b) shows the temperature dependence of the magnetization and the cTPQ method also reproduces the results of the full exact diagonalization.

We show the temperature dependence of the thermal Hall conductivity  $\kappa$  in Fig. 18(c). The thermal Hall conductivity  $\kappa$  at  $|h| = 0.04$  becomes negative below  $T \leq 10^{-2}$ . This negative  $\kappa$  may also be caused by the finite size effects due to the short length of the edges. In fact,  $\kappa$  becomes positive for larger system sizes as we show above. The cTPQ method well reproduces this peculiar temperature dependence. At  $h = 0.08$ ,  $\kappa$  shows a single peak structure and it is also well reproduced by the cTPQ method. These consistencies with the results by the full diagonalization demonstrate the validity of the cTPQ method.

## Appendix C: Comparison between tensor network method and thermal pure quantum state

In this section, we examine the accuracy of the XTRG method, by comparing the results of the cTPQ method with those of the XTRG for  $(L, L') = (6, 2)$  cluster ( $N_s = 24$ ). Fig. 19(a) shows the temperature dependence of the specific heat. We find that both methods reproduce the two-peak structure in the specific heat, which is a characteristic feature in the Kitaev model. Except for the small discrepancy around the low-temperature peak at  $h = 0.04$ , both methods agree well with each other over the three magnitudes of the temperature scale. This consistency demonstrates that the XTRG method with sufficiently large bond dimension gives accurate results.

In Fig. 19(b), we show the temperature dependence of the magnetization. In all the temperature regions, we find that both methods agree well within the error bars. Since the magnetization is given by the first derivative of the free energy, its fluctuation is expected to be small. This may be the reason why the error bars of the magnetization are smaller than those of the specific heat and the thermal Hall conductivity.

We show the temperature dependence of  $\kappa$  in Fig. 19(c) and find that  $D = 500$  already gives sufficiently accurate results of the thermal Hall conductivity  $\kappa$  except for the small deviations on the peak values of  $\kappa$ . This result indicates that the XTRG calculations shown in this paper correctly capture the essence of the thermal Hall conductivity in the extended Kitaev models.

- 
- [1] A. Kitaev, Anyons in an exactly solved model and beyond, *Ann. Phys. (N. Y.)* **321**, 2 (2006).
- [2] Y. Kasahara, T. Ohnishi, Y. Mizukami, O. Tanaka, S. Ma, K. Sugii, N. Kurita, H. Tanaka, J. Nasu, Y. Motome, T. Shibauchi, and Y. Matsuda, Majorana quantization and half-integer thermal quantum Hall effect in a Kitaev spin liquid, *Nature* **559**, 227 (2018).
- [3] J. A. Sears, M. Songvilay, K. W. Plumb, J. P. Clancy,

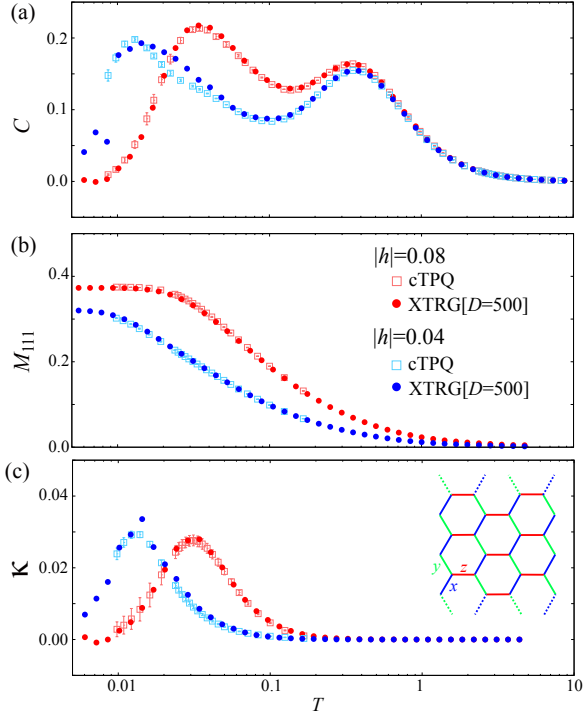


FIG. 19. Temperature dependence of (a) the specific heat, (b) the total magnetization, and (c) the thermal Hall conductivity  $\kappa$ . In the bootstrap sampling, we take 100 independent initial states, and choose 100 samples 50 times with replacement to evaluate the average values and the error vars.

Y. Qiu, Y. Zhao, D. Parshall, and Y.-J. Kim, Magnetic order in  $\alpha$ -rucl<sub>3</sub>: A honeycomb-lattice quantum magnet with strong spin-orbit coupling, *Phys. Rev. B* **91**, 144420 (2015).

- [4] R. D. Johnson, S. C. Williams, A. A. Haghaghirad, J. Singleton, V. Zapf, P. Manuel, I. I. Mazin, Y. Li, H. O. Jeschke, R. Valentí, and R. Coldea, Monoclinic crystal structure of  $\alpha$ -rucl<sub>3</sub> and the zigzag antiferromagnetic ground state, *Phys. Rev. B* **92**, 235119 (2015).
- [5] H. B. Cao, A. Banerjee, J.-Q. Yan, C. A. Bridges, M. D. Lumsden, D. G. Mandrus, D. A. Tennant, B. C. Chakoumakos, and S. E. Nagler, Low-temperature crystal and magnetic structure of  $\alpha$ -rucl<sub>3</sub>, *Phys. Rev. B* **93**, 134423 (2016).
- [6] A. Banerjee, P. Lampen-Kelley, J. Knolle, C. Balz, A. A. Aczel, B. Winn, Y. Liu, D. Pajerowski, J. Yan, C. A. Bridges, *et al.*, Excitations in the field-induced quantum spin liquid state of  $\alpha$ -rucl<sub>3</sub>, *npj Quantum Materials* **3**, 8 (2018).
- [7] M. Yamashita, J. Gouchi, Y. Uwatoko, N. Kurita, and H. Tanaka, Sample dependence of half-integer quantized thermal Hall effect in the Kitaev spin-liquid candidate  $\alpha$ -RuCl<sub>3</sub>, *Phys. Rev. B* **102**, 220404 (2020).
- [8] T. Yokoi, S. Ma, Y. Kasahara, S. Kasahara, T. Shibauchi, N. Kurita, H. Tanaka, J. Nasu, Y. Motome, C. Hickey, S. Trebst, and Y. Matsuda, Half-integer quantized anomalous thermal Hall effect in the Kitaev material candidate  $\alpha$ -RuCl<sub>3</sub>, *Science* **373**, 568 (2021).
- [9] J. Bruin, R. Claus, Y. Matsumoto, N. Kurita, H. Tanaka,

and H. Takagi, Robustness of the thermal hall effect close to half-quantization in  $\alpha$ -rucl<sub>3</sub>, *Nature Physics* **18**, 401 (2022).

- [10] M. Ye, G. B. Halász, L. Savary, and L. Balents, Quantization of the thermal hall conductivity at small hall angles, *Phys. Rev. Lett.* **121**, 147201 (2018).
- [11] Y. Vinkler-Aviv and A. Rosch, Approximately quantized thermal hall effect of chiral liquids coupled to phonons, *Phys. Rev. X* **8**, 031032 (2018).
- [12] A. P. Joy and A. Rosch, Dynamics of visons and thermal hall effect in perturbed kitaev models, *Phys. Rev. X* **12**, 041004 (2022).
- [13] J. Chaloupka, G. Jackeli, and G. Khaliullin, Kitaev-Heisenberg Model on a Honeycomb Lattice: Possible Exotic Phases in Iridium Oxides  $A_2\text{IrO}_3$ , *Phys. Rev. Lett.* **105**, 027204 (2010).
- [14] J. Chaloupka, G. Jackeli, and G. Khaliullin, Zigzag Magnetic Order in the Iridium Oxide  $\text{Na}_2\text{IrO}_3$ , *Phys. Rev. Lett.* **110**, 097204 (2013).
- [15] J. G. Rau, E. K.-H. Lee, and H.-Y. Kee, Generic spin model for the honeycomb iridates beyond the kitaev limit, *Phys. Rev. Lett.* **112**, 077204 (2014).
- [16] J. G. Rau and H.-Y. Kee, Trigonal distortion in the honeycomb iridates: Proximity of zigzag and spiral phases in  $\text{Na}_2\text{IrO}_3$  (2014).
- [17] S. M. Winter, Y. Li, H. O. Jeschke, and R. Valentí, Challenges in design of kitaev materials: Magnetic interactions from competing energy scales, *Phys. Rev. B* **93**, 214431 (2016).
- [18] D. Takikawa and S. Fujimoto, Topological phase transition to abelian anyon phases due to off-diagonal exchange interaction in the kitaev spin liquid state, *Phys. Rev. B* **102**, 174414 (2020).
- [19] M. G. Yamada and S. Fujimoto, Quantum liquid crystals in the finite-field  $k\gamma$  model for  $\alpha$ -rucl<sub>3</sub> (2021).
- [20] P. Czajka, T. Gao, M. Hirschberger, P. Lampen-Kelley, A. Banerjee, J. Yan, D. G. Mandrus, S. E. Nagler, and N. Ong, Oscillations of the thermal conductivity in the spin-liquid state of  $\alpha$ -rucl<sub>3</sub>, *Nature Physics* **17**, 915 (2021).
- [21] P. Czajka, T. Gao, M. Hirschberger, P. Lampen-Kelley, A. Banerjee, N. Quirk, D. G. Mandrus, S. E. Nagler, and N. P. Ong, Planar thermal hall effect of topological bosons in the kitaev magnet  $\alpha$ -rucl<sub>3</sub>, *Nature Materials* **22**, 36 (2023).
- [22] R. Henrich, M. Roslova, A. Isaeva, T. Doert, W. Brenig, B. Büchner, and C. Hess, Large thermal hall effect in  $\alpha$ -rucl<sub>3</sub>: Evidence for heat transport by kitaev-heisenberg paramagnons, *Phys. Rev. B* **99**, 085136 (2019).
- [23] E. Lefrançois, G. Grissonnanche, J. Baglo, P. Lampen-Kelley, J.-Q. Yan, C. Balz, D. Mandrus, S. E. Nagler, S. Kim, Y.-J. Kim, N. Doiron-Leyraud, and L. Taillefer, Evidence of a phonon hall effect in the kitaev spin liquid candidate  $\alpha$ -rucl<sub>3</sub>, *Phys. Rev. X* **12**, 021025 (2022).
- [24] J. Nasu, M. Udagawa, and Y. Motome, Vaporization of kitaev spin liquids, *Phys. Rev. Lett.* **113**, 197205 (2014).
- [25] J. Nasu, M. Udagawa, and Y. Motome, Thermal fractionalization of quantum spins in a kitaev model: Temperature-linear specific heat and coherent transport of majorana fermions, *Phys. Rev. B* **92**, 115122 (2015).
- [26] J. Nasu, J. Yoshitake, and Y. Motome, Thermal transport in the kitaev model, *Phys. Rev. Lett.* **119**, 127204 (2017).

- [27] P. A. McClarty, X.-Y. Dong, M. Gohlke, J. G. Rau, F. Pollmann, R. Moessner, and K. Penc, Topological magnons in kitaev magnets at high fields, *Phys. Rev. B* **98**, 060404 (2018).
- [28] D. G. Joshi, Topological excitations in the ferromagnetic kitaev-heisenberg model, *Phys. Rev. B* **98**, 060405 (2018).
- [29] G. Jackeli and G. Khaliullin, Mott Insulators in the Strong Spin-Orbit Coupling Limit: From Heisenberg to a Quantum Compass and Kitaev Models, *Phys. Rev. Lett.* **102**, 017205 (2009).
- [30] Y. Yamaji, Y. Nomura, M. Kurita, R. Arita, and M. Imada, First-principles study of the honeycomb-lattice iridates  $\text{Na}_2\text{IrO}_3$  in the presence of strong spin-orbit interaction and electron correlations, *Phys. Rev. Lett.* **113**, 107201 (2014).
- [31] S. M. Winter, A. A. Tsirlin, M. Daghofer, J. van den Brink, Y. Singh, P. Gegenwart, and R. Valentí, Models and materials for generalized kitaev magnetism, *J. Phys.: Condens. Matter* **29**, 493002 (2017).
- [32] Y. Yamaji, T. Suzuki, T. Yamada, S.-i. Suga, N. Kawashima, and M. Imada, Clues and criteria for designing a kitaev spin liquid revealed by thermal and spin excitations of the honeycomb iridate  $\text{Na}_2\text{IrO}_3$ , *Phys. Rev. B* **93**, 174425 (2016).
- [33] T. Suzuki and S.-i. Suga, Effective model with strong kitaev interactions for  $\alpha\text{-RuCl}_3$ , *Phys. Rev. B* **97**, 134424 (2018).
- [34] P. Laurell and S. Okamoto, Dynamical and thermal magnetic properties of the kitaev spin liquid candidate  $\alpha\text{-RuCl}_3$ , *npj Quantum Materials* **5**, 1 (2020).
- [35] P. A. Maksimov and A. L. Chernyshev, Rethinking  $\alpha\text{-RuCl}_3$ , *Phys. Rev. Res.* **2**, 033011 (2020).
- [36] A. Catuneanu, Y. Yamaji, G. Wachtel, Y. B. Kim, and H.-Y. Kee, Path to stable quantum spin liquids in spin-orbit coupled correlated materials, *npj Quantum Materials* **3**, 23 (2018).
- [37] T. Yamada, T. Suzuki, and S.-i. Suga, Ground-state properties of the  $k - \Gamma$  model on a honeycomb lattice, *Phys. Rev. B* **102**, 024415 (2020).
- [38] M. Gohlke, G. Wachtel, Y. Yamaji, F. Pollmann, and Y. B. Kim, Quantum spin liquid signatures in kitaev-like frustrated magnets, *Phys. Rev. B* **97**, 075126 (2018).
- [39] H.-Y. Lee, R. Kaneko, L. E. Chern, T. Okubo, Y. Yamaji, N. Kawashima, and Y. B. Kim, Magnetic field induced quantum phases in a tensor network study of kitaev magnets, *Nature communications* **11**, 1639 (2020).
- [40] X.-Y. Zhang, S. Liang, H.-J. Liao, W. Li, and L. Wang, Differentiable programming tensor networks for kitaev magnets, *Phys. Rev. B* **108**, 085103 (2023).
- [41] S.-S. Zhang, G. B. Halász, W. Zhu, and C. D. Batista, Variational study of the kitaev-heisenberg-gamma model, *Phys. Rev. B* **104**, 014411 (2021).
- [42] R. L. Smit, S. Keupert, O. Tsypliyatayev, P. A. Maksimov, A. L. Chernyshev, and P. Kopietz, Magnon damping in the zigzag phase of the kitaev-heisenberg- $\Gamma$  model on a honeycomb lattice, *Phys. Rev. B* **101**, 054424 (2020).
- [43] A. Rayyan, Q. Luo, and H.-Y. Kee, Extent of frustration in the classical kitaev- $\Gamma$  model via bond anisotropy, *Phys. Rev. B* **104**, 094431 (2021).
- [44] Q. Luo, P. P. Stavropoulos, J. S. Gordon, and H.-Y. Kee, Spontaneous chiral-spin ordering in spin-orbit coupled honeycomb magnets, *Phys. Rev. Res.* **4**, 013062 (2022).
- [45] Q. Luo and H.-Y. Kee, Interplay of magnetic field and trigonal distortion in the honeycomb  $\Gamma$  model: Occurrence of a spin-flop phase, *Phys. Rev. B* **105**, 174435 (2022).
- [46] J. Rusnáčko, D. Gotfrýd, and J. c. v. Chaloupka, Kitaev-like honeycomb magnets: Global phase behavior and emergent effective models, *Phys. Rev. B* **99**, 064425 (2019).
- [47] J. S. Gordon, A. Catuneanu, E. S. Sørensen, and H.-Y. Kee, Theory of the field-revealed kitaev spin liquid, *Nature communications* **10**, 1 (2019).
- [48] L. E. Chern, R. Kaneko, H.-Y. Lee, and Y. B. Kim, Magnetic field induced competing phases in spin-orbital entangled kitaev magnets, *Phys. Rev. Res.* **2**, 013014 (2020).
- [49] H. Katsura, N. Nagaosa, and P. A. Lee, Theory of the thermal hall effect in quantum magnets, *Phys. Rev. Lett.* **104**, 066403 (2010).
- [50] A. Kumar and V. Tripathi, Thermal hall conductivity near field-suppressed magnetic order in a kitaev-heisenberg model, arXiv preprint arXiv:2208.13708 <https://doi.org/10.48550/arXiv.2208.13708> (2022).
- [51] B. B. Chen, L. Chen, Z. Chen, W. Li, and A. Weichselbaum, Exponential Thermal Tensor Network Approach for Quantum Lattice Models, *Phys. Rev. X* **8**, 31082 (2018).
- [52] H. Li, D.-W. Qu, H.-K. Zhang, Y.-Z. Jia, S.-S. Gong, Y. Qi, and W. Li, Universal thermodynamics in the Kitaev fractional liquid, *Phys. Rev. Res.* **2**, 043015 (2020), 2006.02405.
- [53] S. Sugiura and A. Shimizu, Canonical thermal pure quantum state, *Phys. Rev. Lett.* **111**, 010401 (2013).
- [54] M. Imada and M. Takahashi, Quantum transfer monte carlo method for finite temperature properties and quantum molecular dynamics method for dynamical correlation functions, *J. Phys. Soc. Jpn.* **55**, 3354 (1986).
- [55] J. Jaklić and P. Prelovšek, Lanczos method for the calculation of finite-temperature quantities in correlated systems, *Phys. Rev. B* **49**, 5065 (1994).
- [56] A. Hams and H. De Raedt, Fast algorithm for finding the eigenvalue distribution of very large matrices, *Phys. Rev. E* **62**, 4365 (2000).
- [57] S. Lloyd, Pure state quantum statistical mechanics and black holes, arXiv:1307.0378 <https://doi.org/10.48550/arXiv.1307.0378>.
- [58] M. Kawamura, K. Yoshimi, T. Misawa, Y. Yamaji, S. Todo, and N. Kawashima, Quantum lattice model solver  $H\Phi$ , *Computer Physics Communications* **217**, 180 (2017).
- [59] K. Ido, M. Kawamura, Y. Motoyama, K. Yoshimi, Y. Yamaji, S. Todo, N. Kawashima, and T. Misawa, Update of  $H\Phi$ : Newly added functions and methods in versions 2 and 3, arXiv preprint arXiv:2307.13222 <https://doi.org/10.48550/arXiv.2307.13222> (2023).
- [60] <https://github.com/issp-center-dev/HPhi/releases>.
- [61] K. Hukushima and K. Nemoto, Exchange Monte Carlo Method and Application to Spin Glass Simulations, *J. Phys. Soc. Japan* **65**, 1604 (1996).
- [62] Z. Zhu, I. Kimchi, D. N. Sheng, and L. Fu, Robust non-abelian spin liquid and a possible intermediate phase in the antiferromagnetic kitaev model with magnetic field, *Phys. Rev. B* **97**, 241110 (2018).
- [63] H.-Y. Lee, R. Kaneko, L. E. Chern, T. Okubo, Y. Yamaji, N. Kawashima, and Y. B. Kim, Magnetic field induced quantum phases in a tensor network study of kitaev mag-

- nets, *Nature Communications* **11**, 1639 (2020).
- [64] P. A. McClarty, X.-Y. Dong, M. Gohlke, J. G. Rau, F. Pollmann, R. Moessner, and K. Penc, Topological magnons in kitaev magnets at high fields, *Phys. Rev. B* **98**, 060404 (2018).
- [65] D. G. Joshi, Topological excitations in the ferromagnetic kitaev-heisenberg model, *Phys. Rev. B* **98**, 060405 (2018).
- [66] L. E. Chern, E. Z. Zhang, and Y. B. Kim, Sign structure of thermal hall conductivity and topological magnons for in-plane field polarized kitaev magnets, *Phys. Rev. Lett.* **126**, 147201 (2021).
- [67] D. Takikawa and S. Fujimoto, Topological phase transition to abelian anyon phases due to off-diagonal exchange interaction in the kitaev spin liquid state, *Phys. Rev. B* **102**, 174414 (2020).
- [68] E. Sela, H.-C. Jiang, M. H. Gerlach, and S. Trebst, Order-by-disorder and spin-orbital liquids in a distorted heisenberg-kitaev model, *Phys. Rev. B* **90**, 035113 (2014).
- [69] T. Suzuki and Y. Yamaji, Thermal properties of spin-s kitaev-heisenberg model on a honeycomb lattice, *Physica B: Condensed Matter* **536**, 637 (2018).
- [70] M. Gohlke, G. Wachtel, Y. Yamaji, F. Pollmann, and Y. B. Kim, Quantum spin liquid signatures in kitaev-like frustrated magnets, *Phys. Rev. B* **97**, 075126 (2018).
- [71] L. S. Blackford, J. Choi, A. Cleary, E. D'Azevedo, J. Demmel, I. Dhillon, J. Dongarra, S. Hammarling, G. Henry, A. Petitet, K. Stanley, D. Walker, and R. C. Whaley, *ScaLAPACK Users' Guide* (Society for Industrial and Applied Mathematics, Philadelphia, PA, 1997).